Increased glycolysis affects β-cell function and identity in aging and diabetes

Naoya Murao [1], Norihide Yokoi [1,2], Harumi Takahashi [1,*], Tomohide Hayami [1,3], Yasuhiro Minami [4], Susumu Seino [1]

ABSTRACT

Objective: Age is a risk factor for type 2 diabetes (T2D). We aimed to elucidate whether β-cell glucose metabolism is altered with aging and contributes to T2D.
Methods: We used senescence-accelerated mice (SAM), C57BL/6J (B6) mice, and *ob/ob* mice as aging models. As a diabetes model, we used *db/db* mice. The glucose responsiveness of insulin secretion and the [U-^{13}C]-glucose metabolic flux were examined in isolated islets. We analyzed the expression of β-cell-specific genes in isolated islets and pancreatic sections as molecular signatures of β-cell identity. β cells defective in the malate-aspartate (MA) shuttle were previously generated from MIN6-K8 cells by the knockout of *Got1*, a component of the shuttle. We analyzed *Got1* KO β cells as a model of increased glycolysis.
Results: We identified hyperresponsiveness to glucose and compromised cellular identity as dysfunctional phenotypes shared in common between aged and diabetic mouse β cells. We also observed a metabolic commonality between aged and diabetic β cells: hyperactive glycolysis through the increased expression of nicotinamide mononucleotide adenylyl transferase 2 (*Nmnat2*), a cytosolic nicotinamide adenine dinucleotide (NAD)-synthesizing enzyme. *Got1* KO β cells showed increased glycolysis, β-cell dysfunction, and impaired cellular identity, phenocopying aging and diabetes. Using *Got1* KO β cells, we show that attenuation of glycolysis or Nmnat2 activity can restore β-cell function and identity.
Conclusions: Our study demonstrates that hyperactive glycolysis is a metabolic signature of aged and diabetic β cells, which may underlie age-related β-cell dysfunction and loss of cellular identity. We suggest Nmnat2 suppression as an approach to counteract age-related T2D.

1. INTRODUCTION

Pancreatic β cells sense elevated blood glucose and in response secrete insulin to maintain blood glucose levels within narrow limits. Glucose-induced insulin secretion (GIIS) is regulated by two signaling pathways, the triggering and amplifying pathways, both of which require β-cell glucose metabolism [1]. The triggering pathway is characterized by an increase in the intracellular ATP levels, which causes an inhibition of the ATP-sensitive K$^+$ (K$_{ATP}$) channels, resulting in membrane depolarization and the opening of voltage-dependent Ca^{2+} channels, which increases intracellular [Ca^{2+}], thereby stimulating insulin granule exocytosis. The amplifying pathway enhances the triggering pathway by other metabolic signals derived from glucose metabolism [2]. Thus, β-cell glucose metabolism is central to the regulation of GIIS.

In type 2 diabetes (T2D), β cells fail to secrete sufficient insulin to compensate for insulin resistance or nutrient excess, leading to hyperglycemia [3]. Given that the prevalence of T2D increases with aging, peaking in the seventh/eighth decades of life [4], it has been suggested that an age-associated decline in β-cell function underlies T2D. This issue has been addressed in humans, but the studies display variability in the outcomes [5].

Surprisingly, in rodent models, it has been shown that insulin secretion is enhanced with aging [6—10], and it has been attributed to various factors, including epigenetic activation of β-cell function [7], reduced K$_{ATP}$ channel conductance [8], and p16-mediated cellular senescence [9]. Although these studies highlight the beneficial aspects of these age-associated changes to maintain glucose homeostasis, several questions remain unaddressed. First, previous studies dealing with the age-associated changes in β cells were mostly carried out on C57BL/6 (B6)-related strains, and it cannot be ruled out that the changes are strain specific. Second, there is a lack of evidence on whether glucose metabolism is altered in aged β cells. Finally, it is unclear how increased insulin secretion in aged β cells would lead to T2D. To

[1]Division of Molecular and Metabolic Medicine, Graduate School of Medicine, Kobe University, 7-5-1 Kusunoki-cho, Chuo-ku, Kobe, Hyogo 650-0017, Japan [2]Laboratory of Animal Breeding and Genetics, Graduate School of Agriculture, Kyoto University, Sakyo-ku, Kyoto, Kyoto 606-8502, Japan [3]Division of Diabetes, Department of Internal Medicine, Aichi Medical University, Nagakute, Aichi 480-1195, Japan [4]Division of Cell Physiology, Graduate School of Medicine, Kobe University, Chuo-ku, Kobe, Hyogo 650-0017, Japan

*Corresponding author. E-mail: htakahashi@puppy.kobe-u.ac.jp (H. Takahashi).

Original Article

address these issues, we studied various models of aging (senescence-accelerated mice; SAM, B6, and *ob*/*ob* mice) and diabetes (*db*/*db* mice), as well as clonal β cell lines, with a focus on glucose metabolism.

The SAM include sub-strains with various degrees of senescence and lifespans. The SAMP and SAMR strains were derived from a mixed AKR/J strain by selective inbreeding for and against spontaneous early senescence, respectively [11,12]. Although they have no specific genetic modification, each strain has unique nucleotide polymorphisms [13]. SAMP1 is a model of premature senescence, with a spectrum of changes in the cardiovascular, renal, and nervous systems, as compared with a control strain SAM-resistant 1 (SAMR1) [14—16]. These pathophysiological traits are also observed in elderly humans. Metabolically, SAMP1 exhibits early reduction in exercise performance and energy expenditure along with decreased fatty acid oxidation in the muscle and liver, mimicking the decline in systemic metabolism seen in elderly humans [17]. The activities of Cu/Zn-superoxide dismutase [18] and uncoupling protein 1 (Ucp1) are decreased in SAMP1 [18,19]. Due to these defects in the mitochondrial function, SAMP1 exhibits increased oxidative stress in various organs [18,20,21] and has been used to test antioxidants [22,23].

So far, glucose metabolism and β-cell function in SAM have been poorly explored. In the present study, we show that β cells in SAM exhibit age-associated changes that closely recapitulate other mouse strains. Our results demonstrate that glycolysis is increased in aged as well as in diabetic β cells and that hyperactive glycolysis adversely affects β-cell function and identity, suggesting that aging could contribute to the development of T2D. We identified nicotinamide mononucleotide adenylyl transferase 2 (Nmnat2), a cytosolic nicotinamide adenine dinucleotide (NAD)-synthesizing enzyme, as a key mediator of β-cell dysfunction by hyperactive glycolysis.

2. MATERIALS AND METHODS

Details on the reagents and resources can be found in Supplementary File 1.

2.1. Mice and diets

All mice were purchased from the vendors listed in Supplementary File 1 at 5—12 weeks of age and maintained until experiments. Middle-aged and aged C57BL/6JJcl mice were also provided by the vendor at 1 year and 2 years of age, respectively. The mice were maintained under specific-pathogen-free conditions at $23 \pm 2\ °C$ and $55 \pm 10\%$ relative humidity in 12-h light—dark cycles, with free access to water and standard chow CE-2 (CLEA Japan). The health status of the mice was checked regularly. Ad libitum-fed blood glucose levels were measured at 8 a.m. All experiments were performed using male mice. The age and number of mice analyzed is detailed in the figure legends. All in vivo experiments were performed with the approval of the Committee on Animal Experimentation of Kobe University, complying with the Guidelines for Animal Experimentation at Kobe University and current Japanese legislation. Male mice were used in all the experiments.

2.2. Cell lines

MIN6-K8 cells were established as described previously [24]. *Got1* KO-1 and -2 cells were established by sub-cloning of MIN6-K8 cells transfected with Cas9 nickase and guide RNA pairs targeting mouse *Got1* as described previously [25]. *Got1* KO-1 and -2 cells refer to clones A60 and A64, in Murao et al. [25], respectively. MIN6-K8 and *Got1* KO cells were cultured in Dulbecco's Modified Eagle Medium

(high glucose) (DMEM-HG, Sigma) containing 4500 mg/L glucose supplemented with 10% fetal bovine serum (FBS) (BioWest) and 5 ppm 2-mercaptoethanol. For treatment with HG, LD, or 2DG (Figure 6A, Supplementary Table 5), the respective culture media were prepared by adding glucose, L-glutamine, and 2-deoxy-D-glucose (2DG) (Wako) to DMEM without glucose (Sigma) according to the manufacturer's instructions. AD293 cells were purchased from Agilent and cultured in DMEM supplemented with 10% FBS, 1 mM sodium pyruvate, and 5 ppm 2-mercaptoethanol. All cells were maintained at $37\ °C$ with 5% CO_2.

2.3. Mouse pancreatic islets

The pancreas was digested following intraductal injection of Hanks' balanced salt solution (HBSS) supplemented with collagenase P. The islets were transferred to 60-mm nontreated plates (Iwaki) and cultured overnight in RPMI-1640 (Sigma) supplemented with 10% FBS and 1% penicillin—streptomycin solution (Wako) at $37\ °C$ with 5% CO_2 before the experiments.

2.4. Oral glucose tolerance test

Experiments were performed as described in Oduori et al. [26] with slight modifications. Briefly, mice were fasted for 5 h (8 a.m.—1 p.m.) before the experiments. Glucose was dissolved in sterile water and orally administered at a dose of 1.5 g/kg body weight. Blood samples were obtained from the tail vein. Blood glucose levels were measured using the Antsense Duo glucose analyzer (Horiba). For insulin measurement, blood was collected using heparinized capillaries, added with EDTA (to the final concentration of 2 mM) and aprotinin (to the final concentration of 500 KIU/mL), and centrifuged at $2000 \times g$, $4\ °C$ for 20 min to obtain plasma. Insulin was quantified by Ultra Sensitive Mouse/Rat Insulin ELISA (Morinaga) according to the manufacturer's instructions.

2.5. Intraperitoneal insulin tolerance test

Mice were fasted for 5 h (8 a.m.—1 p.m.) before the experiments. Humulin R (Lilly) was diluted with saline and intraperitoneally injected at a dose of 0.75 unit/kg body weight. Blood samples were obtained from the tail vein. Blood glucose levels were measured by the Antsense Duo glucose analyzer.

2.6. Insulin secretion and content in pancreatic islets

The experiments were performed as described in Oduori et al. [26] with slight modifications. Briefly, overnight-cultured islets were rinsed twice with Krebs—Ringer bicarbonate buffer supplemented with 10 mM HEPES and 0.1% BSA (KRBH) containing 2.8 mM glucose (2.8G-KRBH), followed by preincubation with 2.8G-KRBH for 30 min at $37\ °C$. Alternatively, islets designated for stimulation with 0.1 and 1.0 mM glucose were preincubated with the same glucose concentration as the stimulation. The islets were then rinsed with 2.8G-KRBH and transferred to a round-bottom 96-well plate (Corning) at 1 islet/ well. 100 µL/well of KRBH containing various concentrations of glucose was added and incubated for 30 min at $37\ °C$. The reaction was quenched by cooling the plate on ice for 10 min, after which 50 µL/well of the supernatant was collected for the measurement of released insulin. The islets were then extracted by adding 50 µL/well of KRBH containing 0.1% Triton-X, followed by a freeze-thaw at $-80\ °C$ for measurement of the remaining insulin. Insulin in the supernatant and extract were quantified by homogeneous time-resolved fluorescence assay (HTRF) Insulin Ultrasensitive kit (Cisbio) according to the manufacturer's instructions. The insulin content was determined as the sum of insulin in the supernatant and the extract.

Insulin secretion was expressed as the percentage of released insulin in insulin content. Total DNA in the extract was measured by PicoGreen dsDNA assay (Thermo), according to the manufacturer's instructions.

2.7. Insulin secretion and content in cell lines

The experiments were performed as described in Oduori et al. [26] with slight modifications. Briefly, cells were seeded in 24-well plates at 5×10^5 cells/well and cultured for 48 h as described above. Alternatively, cells were cultured and infected with adenoviruses as described in section 2.14. The cells were then rinsed 3 times and pre-incubated for 30 min with 300 μL/well of 2.8G-KRBH. Alternatively, cells designated for stimulation with 0.1 mM glucose were pre-incubated with the same glucose concentration as the stimulation. Cells were then rinsed with 2.8G-KRBH and supernatant was replaced with 300 μL/well of KRBH containing various concentrations of glucose, followed by 30-min incubation at 37 °C. The reaction was quenched by cooling the plate on ice for 10 min, after which the whole supernatant was collected for the measurement of released insulin. Cells were then extracted by adding 300 μL/well of KRBH containing 0.1% Triton-X and shaking the plate for 15 min. Insulin release, insulin content, and DNA were quantified as described in section 2.6.

2.8. RT-qPCR

Cells were cultured under the following conditions: (1) to determinate relative gene expression in *Got1* KO cells (Figure 5B and F, Supplementary Table 4), the cells were seeded in 6-well plates at 2×10^6 cells/well and cultured for 48 h; (2) for treatment with HG, LD, or 2DG (Figure 6A, Supplementary Table 5), the cells were seeded in 6-well plates at 7×10^5 cells/well and cultured for 48 h in DMEM-HG. The culture media was then replaced with HG, LD, or 2DG prepared as described in section 2.2., and the cells were cultured for another 4 days; (3) for *Nmnat2* knockdown (Figure 6C, Supplementary Table 6), the cells were cultured and infected with adenoviruses as described in section 2.14. Total RNA samples were prepared from overnight-cultured islets or cells using RNeasy Micro or RNeasy mini kits (Qiagen), respectively, according to the manufacturer's instructions. RNase-free DNase set (Qiagen) was used to digest DNA. cDNA was prepared using the ReverTraAce qPCR RT kit (Toyobo) according to the manufacturer's instructions. Quantitative real-time PCR reactions were performed on the StepOnePlus Real-Time PCR System (Thermo) using TaqMan Universal Master Mix II with UNG and Taqman probes (Thermo). The probe details are described in Supplementary File 1. The relative gene expression was calculated by the $2^{-\Delta\Delta CT}$ method and normalized to *Tbp*.

2.9. [U-^{13}C]-glucose tracing

For measurement of the metabolites in islets, 100—200 islets were used for each sample. Overnight-cultured islets were rinsed twice with 2.8G-KRBH, followed by preincubation with 2.8G-KRBH for 60 min at 37 °C. The islets were then rinsed with 2.8G-KRBH and incubated with KRBH containing 2.8 mM or 11.1 mM of [U-^{13}C]-glucose (Sigma) for another 60 min at 37 °C. They were then quickly collected onto a 20 μm nylon net filter (Millipore) placed on a paper towel and rinsed with ice-cold 5% aqueous mannitol. Subsequently, they were placed into 2 mL screw tubes containing 500 μL of ice-cold extraction buffer (67.5% methanol, 7.5% chloroform, 25% water) along with the filter, snap-frozen in liquid nitrogen, and stored at −80 °C until extraction of the metabolites.

For measurement of the metabolites in cells, the cells were seeded in 6-well plates at 2×10^6 cells/well and cultured for 48 h. Alternatively, the cells were cultured and infected with adenoviruses as described in

section 2.14. The cells were then rinsed three times with 2.8G-KRBH, followed by preincubation with 2.8G-KRBH for 60 min at 37 °C. The supernatant was replaced with KRBH containing 2.8 mM or 11.1 mM [U-^{13}C]-glucose, followed by incubation for another 30 min at 37 °C, and the supernatant was discarded. The cells were quickly rinsed with ice-cold 5% aqueous mannitol. The whole plate was then snap frozen on liquid nitrogen. The cells were extracted by the addition of 500 μL of ice-cold extraction buffer, thawed on ice, scraped into 2 mL screw tubes along with the supernatant, and stored at −80 °C until the extraction of the metabolites.

Crude samples from islets or cells were added with 80 μL of diluted (1:640) internal standard (Human Metabolome Technologies), 165 μL of methanol, and 465 μL of chloroform. The samples were homogenized by a pre-cooled beads crusher at 3200 rpm for 1 min and centrifuged at $15,000 \times g$ at 4 °C for 3 min. The aqueous layer was transferred to pre-wetted ultrafiltration tubes (Human Metabolome Technologies) and centrifuged at $9100 \times g$ at 4 °C until completely filtered. The filtrate was freeze dried and re-dissolved in 5—10 μL of water, which was then subjected to mass spectrometry. The organic layer was evaporated by decompression at room temperature, and the residue was re-suspended in lysis buffer (see section 2.13.), which was then subjected to BCA protein assay (Thermo).

Metabolites were measured by a G7100A capillary electrophoresis (Agilent) interfaced with a G6224A time-of-flight LC/MS mass spectrometer (Agilent). A G1310A isocratic pump (Agilent) equipped with a G1379B degasser (Agilent) was used to supply sheath liquid (Human Metabolome Technologies). The mass spectrometer was operated in positive ionization mode for the detection of Asp and Glu or in negative ionization mode for the other metabolites. All separations were performed on fused silica capillaries (Human Metabolome Technologies) at 25 °C using appropriate analysis buffer (Human Metabolome Technologies) as the background electrolyte. The applied voltage was set to 27 and 30 kV at 20 °C together with a pressure application of 10 and 15 mbar for positive and negative ionization modes, respectively. The sheath liquid (Human Metabolome Technologies) was delivered to a nebulizer by an isocratic pump (Agilent) at 1 mL/min. Chromatograms and mass spectra were analyzed by MassHunter qualitative analysis (Agilent). Annotation and quantification of chromatogram peaks were carried out by using a standard mixture (Human Metabolome Technologies) as a reference. The abundance of NAD and NADH was normalized to the protein content. ^{13}C enrichment represents the percentage of ^{13}C-labeled carbon in each metabolite pool and was calculated as described in the study by Wortham et al. [27].

2.10. Immunofluorescence staining

For immunofluorescence staining of pancreas, the pancreases were dissected from euthanized mice, washed with phosphate-buffered saline (PBS), and fixed with 10% formalin neutral buffer solution (Wako) overnight at room temperature, followed by dehydration in 70% ethanol for 7 h at room temperature. The fixed pancreas were embedded in paraffin and serial 5-μm sections were cut with a microtome. The pancreatic sections were deparaffinized by the conventional method. In staining for Aldh1a3, MafA, Nkx-6.1, Nmnat2, and Pdx1, antigen retrieval was performed by boiling the deparaffinized pancreatic sections in sodium citrate buffer (10 mM sodium citrate, 0.1% NP-40, pH 6.0) in a microwave oven for 15 min. For immuno-fluorescence staining of cell lines, the cells were seeded on a round cover glass (Matsunami) placed in 12-well plates and cultured for 48 h. The cells were fixed with 3.8% formalin in PBS for 15 min at room temperature. The pancreatic sections or cells were blocked with PBS

supplemented with 10% goat serum and 0.1% Triton-X. Primary antibodies indicated in Supplementary File 1 were diluted with PBS containing 1% goat serum and 0.01% Triton-X at the following concentrations: anti-Aldh1a3 (1:100); anti-Glucagon (1:500); anti-Insulin (Dako, 1:10); anti-MafA (1:100); anti-Nkx-6.1 (1:1200); anti-Nmnat2 (1:200); anti-Pdx1 (1:200); and anti-Somatostatin (1:200). The pancreas sections or cells were loaded with diluted antibodies and incubated overnight at 4 °C. Appropriate fluorescence-conjugated secondary antibodies indicated in Supplementary File 1 were diluted with PBS containing 1% goat serum and 0.01% Triton-X (1:500). The sections were then loaded with diluted secondary antibodies and incubated in the dark for 1 h at room temperature, followed by treatment with DAPI (Dojindo) diluted with PBS (1:2000) in the dark for 3 min at room temperature. The slides were mounted in Fluoromount (Diagnostic BioSystems). Images were taken using a BZ-X810 fluorescence microscope (Keyence).

2.11. Hematoxylin—eosin staining
Deparaffinized pancreatic sections were stained with hematoxylin and eosin by the conventional method. The slides were mounted in malinol (Muto). Images were taken using a BZ-X810 fluorescence microscope (Keyence).

2.12. DAB staining
Pancreatic sections were deparaffinized, blocked, and loaded with anti-insulin (Cell Signaling, 1:400) or anti-CD45 (1:200) antibodies as described in section 2.10. The slides were loaded with anti-rabbit POD conjugate (TaKaRa) and incubated for 30 min at room temperature. The slides were then loaded with DAB substrate solution (Nichirei) and incubated for 30 min at room temperature. The slides were washed with water, counterstained with hematoxylin, dehydrated, and mounted in malinol (Muto). Images were taken using a BZ-X810 fluorescence microscope (Keyence).

2.13. Western blotting
Experiments were performed as described in Ryu et al. [28] with slight modifications. Briefly, the cells were cultured and infected with adenoviral vectors as described in section 2.14. The cells were then washed three times with ice-cold PBS and lysed with 70 μL/well of lysis buffer (20 mM Tris—HCl pH 7.5, 150 mM NaCl, 1 mM EDTA, 1 mM EGTA, 1% NP-40, 1% sodium deoxycholate, 0.1% SDS) containing 5 mM DTT, 25 mM sodium fluoride, 50 μM PJ34 (PARP inhibitor), 50 μM Sirtinol (Sirtuin inhibitor), 0.5 μM PDD00017273 (PARG inhibitor), 1× cOmplete protease inhibitor cocktail (Roche), and 1× PhosSTOP (Sigma).
The cells were then incubated on ice for 30 min for extraction and scraped. The lysate was collected in sample tubes, sonicated for 20 s on ice, and centrifuged at 15,000×g at 4 °C for 30 min. The supernatant was collected, and the protein was quantified by Bradford assay (Bio-Rad). All samples were adjusted to the same protein concentration (40—50 μg/lane), separated on an 8% polyacrylamide-SDS gel, and transferred to a PVDF membrane. The membrane was blocked with 1% nonfat milk in Tris-Buffered Saline with Tween 20 (TBS-T) and incubated with the following primary antibodies in TBS-T supplemented with 1% BSA overnight at 4 °C: anti-acetyl-p53 (Lys379) (1:1000), anti-α-Tubulin (1:1000), anti-p53 (1:1000), anti-PAR (1:4000), anti-Parp1 (1:250), and anti-Sirt1 (1:1000). The membrane was then incubated with anti-rabbit HRP-conjugated IgG (1:1000) or anti-mouse HRP-conjugated IgG (1:1000) in TBS-T supplemented with 1% BSA for 1 h at room temperature. Signals were visualized using an ECL detection reagent (GE Healthcare). Images were taken by ImageQuant LAS 4000 (GE Healthcare) and quantified by ImageJ (version 1.53k, https://imagej.nih.gov/ij/index.html).

2.14. Knockdown of *Nmnat2*
Adenoviral shRNA expression constructs targeting mouse *Nmnat2* mRNA and scramble shRNA were purchased from VectorBuilder. Adenoviruses were generated by transfection of the plasmid constructs into AD293 cells (Agilent) using Lipofectamine 2000 (Thermo). The viruses were collected according to the manufacturer's protocol and purified by using Vivapure AdenoPACK 20 (Sartorius).
For the measurement of insulin secretion and content, the cells were plated in 24-well plates at 2×10^5 cells/well. For the other experiments, the cells were plated in 6-well plates at 4×10^5 cells/well. Following a 4-day culture, the cells were infected with adenoviruses at multiplicity of infection (MOI) of 5. Forty-eight hours after the first infection, the culture medium was discarded and the cells were again infected with the same amount of viruses. Forty-eight hours after the second infection, the cells were subjected to analysis.

2.15. Statistical analysis
Sample sizes were estimated from the expected effect size based on previous experiments. No randomization or blinding was used. For in vivo experiments, n represents the number of mice. For islet [U-^{13}C]-glucose tracing and islet RT-qPCR experiments, n represents the number of biological replicates using islets from different mice. For measurements of islet insulin content and secretion, n represents the number of islets pooled from two mice. For experiments using cell lines, n represents the number of biological replicates using cells grown in different wells. Data are shown as mean ± standard error of the mean (SEM) along with the plot of individual data points. For statistical comparisons of two groups, two-tailed unpaired Welch's unpaired t-test was used. For more than three groups, one-way ANOVA or two-way ANOVA was used followed by pairwise comparisons corrected by Dunnett's or Tukey's method. $P < 0.05$ was considered as statistically significant. Statistical parameters and analyses used are indicated in the figure legends. No statistical methods were used to determine whether the data met the assumptions of the statistical approach. Statistical analyses were performed using GraphPad Prism 9. Heatmaps were generated using Heatmapper (http://www.heatmapper.ca/) [29].

3. RESULTS

3.1. Increased β-cell glucose sensitivity leads to reduced glucose excursions in aged mice
SAMP1 (P1) showed more senescence than SAMR1 (R1), consistent with previous reports [12] (Figure 1A). P1 also showed decreased body weight compared with R1 after 50—60 weeks of age (Supplementary Figure 1A). Ad libitum-fed blood glucose levels were comparable between R1 and P1 throughout their lifespan (Supplementary Figure 1B). Neither strain manifested hyperglycemia (Supplementary Figure 1B). To clarify age-associated changes, we examined young mice (13—30 weeks old) and aged mice (more than 50 weeks old), according to previous studies [14,16,17,22]. We also examined whether young P1 show age-associated changes compared with young R1.
In the fasting state, aged R1 showed lower blood glucose (Supplementary Figure 1C) as well as increased plasma insulin levels compared with young R1 (Figure 1C, 0 min). Oral glucose tolerance tests (OGTT) revealed that (1) glucose excursions were smaller in young P1 than in young R1 and (2) glucose excursions in both R1 and P1 were significantly reduced in aged mice compared with young mice
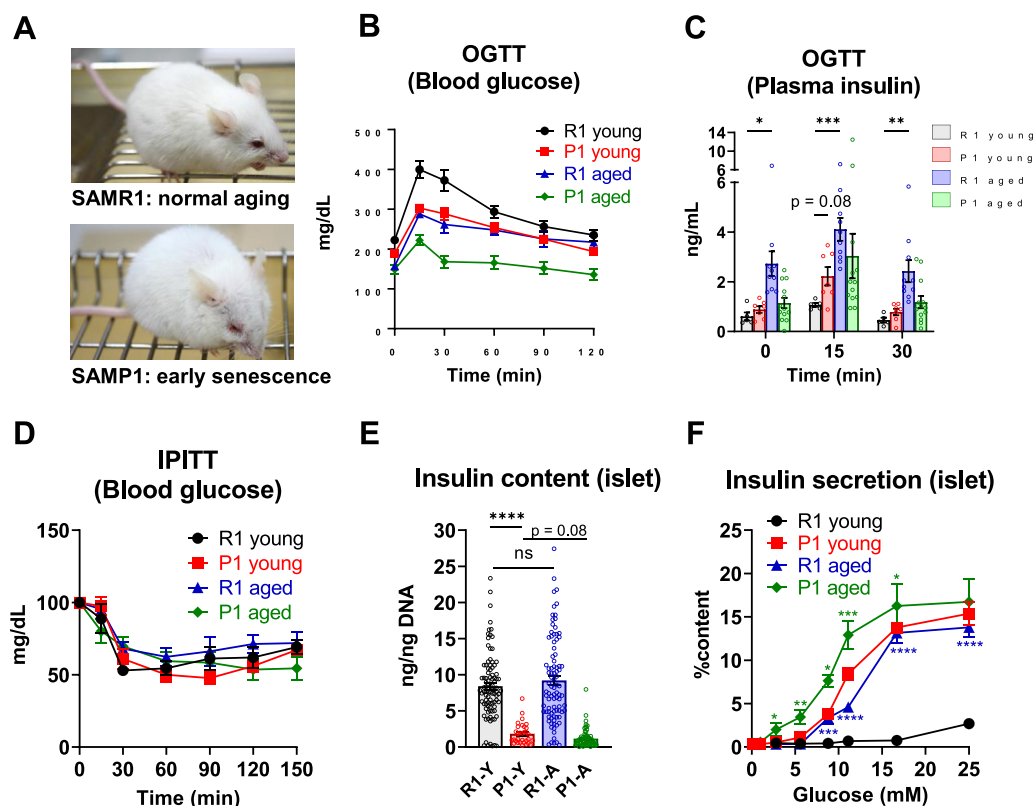
Figure 1: Increased β-cell glucose sensitivity leads to reduced glucose excursions in aged mice. (A) Senescent appearance of aged SAMP1 (67 wks) in comparison with age-matched SAMR1. (B) Oral glucose tolerance test (OGTT). R1 Young (R1-Y): 19 wks, n = 8; P1-Y: 19 wks, n = 12; R1 aged (R1-A): 67 wks, n = 4; P1-A: 67 wks, n = 4. See also Supplementary Figure 1C and D. (C) Plasma insulin levels during OGTT. R1-Y: 17 wks, n = 5; P1-Y: 17 wks, n = 8; R1-A: 76 wks, n = 9; P1-A: 76 wks, n = 13. Statistical comparisons were made by repeated-measures two-way ANOVA with Tukey's post hoc test. (D) Intraperitoneal insulin tolerance test (IPITT). R1-Y: 26 wks, n = 7; P1-Y: 26 wks, n = 8; R1-A: 76 wks, n = 7; P1-A: 76 wks, n = 4. See also Supplementary Figure 1H. (E) Insulin content normalized to the DNA content in islets. R1-Y: 22 wks, n = 94; P1-Y: 32 wks, n = 32; R1-A: 97 wks, n = 91; P1-A: 82 wks, n = 71. Statistical comparisons were made by one-way ANOVA with Dunnett's post hoc test between the indicated pairs. Adjusted p-value is indicated. (F) Dose-dependent effects of glucose on insulin secretion from islets. R1-Y: 22 wks, P1-Y: 32 wks, R1-A: 94 wks, P1-A: 82 wks, n = 10−16 for each. Statistical comparisons were made by Welch's unpaired *t*-test between R1-Y and R1-A, or P1-Y and P1-A. Data are represented as mean ± SEM. *$p < 0.05$, **$p < 0.01$, ***$p < 0.001$, ****$p < 0.0001$, ns: not significant.

(Figure 1B, Supplementary Figure 1D). The same trend was observed during intraperitoneal glucose tolerance tests (IPGTT) (Supplementary Figure 1E and F). Glucose-stimulated plasma insulin levels were substantially increased in aged R1 compared with those in young R1 during OGTT and IPGTT (Figure 1C, Supplementary Figure 1G). Young P1 trended toward higher plasma insulin levels than young R1 during OGTT (Figure 1C). However, aged P1 showed little increase in plasma insulin levels compared with young P1 during OGTT and IPGTT (Figure 1C, Supplementary Figure 1G). The four groups did not show any significant difference in insulin sensitivity as assessed by intraperitoneal insulin tolerance tests (IPITT) (Figure 1D, Supplementary Figure 1H). These results indicate that (1) aging leads to reduced glucose excursions associated with increased plasma insulin in R1 and (2) these age-associated changes are recapitulated in young P1.

Next, we analyzed β cells in these mice. In the whole pancreatic sections, we detected large islets (insulin positive area >3 × 10⁴ μm²) in only aged R1 and aged P1 (Supplementary Figure 2A, red arrows), consistently with a previous report on aged B6 mice [8]. Hematoxylin—eosin (H—E) staining and immunostaining for islet hormones revealed no obvious alterations in islet architecture or cellular composition

(Supplementary Figure 2B). Notably, we observed perivascular infiltration of mononuclear cells in exocrine regions of 59- and 86-week-old P1, which tested positive for CD45 (Supplementary Figure 3, red arrows). This is consistent with a previous report showing infiltration of T-lymphocytes in multiple organs in aged P1 [30].

Although the insulin content was comparable between islets from young R1 and aged R1, the insulin content in young P1 islets was substantially lower than that in young R1 and tended to be further decreased in aged P1 (Figure 1E). The glucose responsiveness of insulin secretion was markedly increased in aged R1 islets compared with that in young R1 (Figure 1F). Young P1 islets also showed elevated glucose responsiveness compared with young R1, which was further increased in aged P1 (Figure 1F). Our findings indicate that increased plasma insulin levels in aged R1 are attributable to elevated β-cell glucose responsiveness along with preserved insulin content, whereas the lack of increase in plasma insulin levels in aged P1 may be due to the decrease in the insulin content.

To further explore the common features of aged β cells of different genetic and metabolic backgrounds, we analyzed C57BL/6J (B6) and obese *ob/ob* mice. Both middle-aged (59 weeks) and aged (110
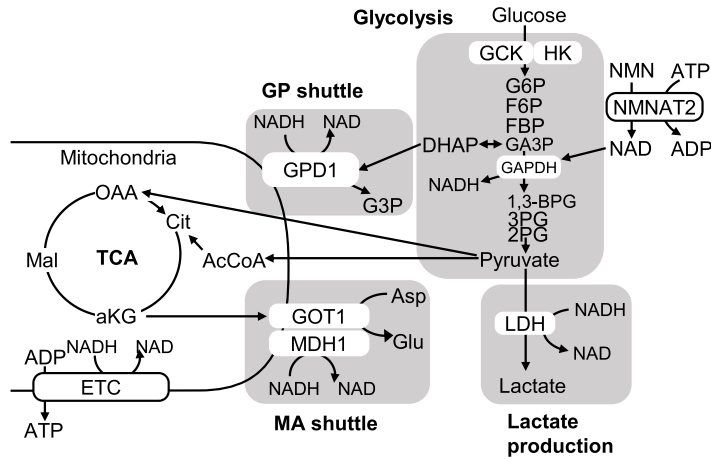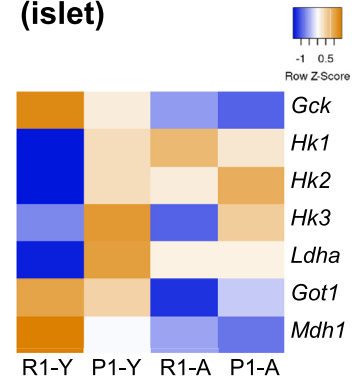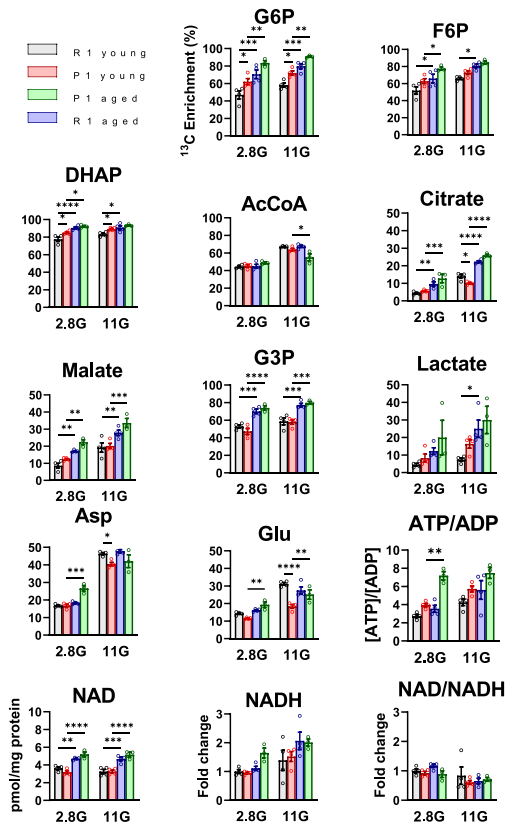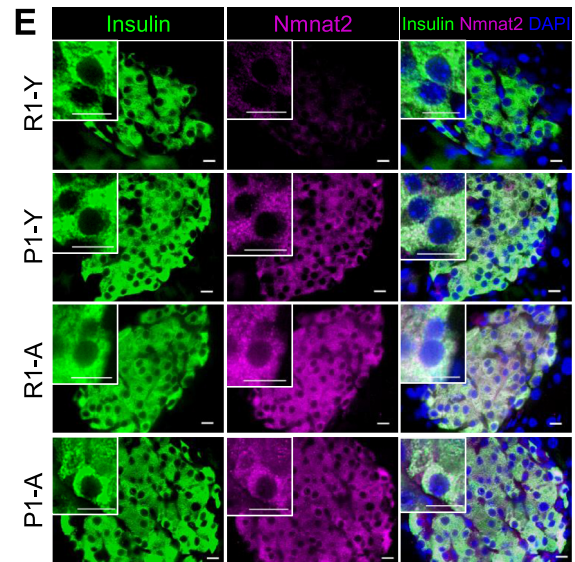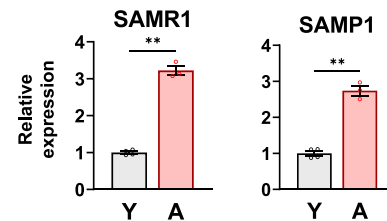
Figure 2: Aged islets show upregulated glucose metabolism and altered cytosolic NAD metabolism. (A) Schematic overview of glucose metabolism. Metabolites and genes assessed in the following experiments are indicated. G6P, glucose 6-phosphate; F6P, fructose 6-phosphate; FBP, fructose 1,6-bisphosphate; GA3P, glyceraldehyde 3-phosphate; DHAP, dihydroxyacetone phosphate; G3P, glycerol 3-phosphate; 1,3-BPG, 1,3-bisphosphoglycerate; 3PG, 3-phosphoglycerate; 2PG, 2-phosphoglycerate; AcCoA, acetyl CoA; Cit, citrate; aKG, α-ketoglutarate; OAA, oxaloacetate; Asp, aspartate; Glu, glutamate; NMN, nicotinamide mononucleotide; ETC, electron transport chain. (B) [U-^{13}C]-glucose tracing experiment in SAM islets. Enrichment of ^{13}C for the indicated metabolites following a 1-h incubation with 2.8 mM (2.8G) or 11.1 mM [U-^{13}C]-glucose (11G) were measured. For NAD and NADH, intracellular content is indicated. R1-Y (25 wks, n = 4), P1-Y (25 wks, n = 4), R1-A (55 wks, n = 4), P1-A (55 wks, n = 3). Statistical comparisons were made by two-way ANOVA with Tukey's post hoc test. See also Supplementary Figure 8A for other metabolites. (C) Expression of metabolic genes in SAM islets assessed by RT-qPCR. Means of each group are visualized. Heatmap scale is Z score for the number of deviations away from the row mean. R1-Y: 27 wks, n = 4; P1-Y: 27 wks, n = 4; R1-A: 97 wks, n = 3; P1-A: 50 wks, n = 3. See Supplementary Table 1 for quantitative values. (D) Expression of *Nmnat2* in islets assessed by RT-qPCR. Statistical comparisons were made by Welch's unpaired *t*-test. R1-Y: 27 wks, n = 4; R1-A: 97 wks, n = 3; P1-Y: 27 wks, n = 4; P1-A: 50 wks, n = 3. (E) Immunofluorescence staining of the pancreatic sections from SAM mice for Insulin (green) and Nmnat2 (magenta). Nuclei were stained with DAPI (blue). R1-Y: 16 wks; P1-Y: 16 wks; R1-A: 84 wks; P1-A: 84 wks. Scale bars, 10 μm. Insets show the representative cells. Data are represented as mean ± SEM for B and D. *p < 0.05, **p < 0.01, ***p < 0.001, ****p < 0.0001.

weeks) B6 mice showed increased body weight compared with young mice (18 weeks) (Supplementary Figure 4A).

OGTT in B6 mice revealed age-dependent reduction in glucose excursions (Supplementary Figure 4B) as well as increased plasma insulin response (Supplementary Figure 4C). There was no significant difference in insulin sensitivity during IPITT despite the increased body weight (Supplementary Figure 4D), which is consistent with a previous report [31]. Aged B6 islets exhibited reduced insulin content as well as a leftward shift of glucose sensitivity (Supplementary Figure 4E and F). There was no significant difference in body weight between young (14 weeks) and aged (96 weeks) *ob/ob* mice, albeit with large variations in the aged mice (Supplementary Figure 5A). OGTT demonstrated a substantial reduction in glucose excursions in aged *ob/ob* mice compared with young *ob/ob* mice that was associated with a trend toward higher plasma insulin response (Supplementary Figure 5B and C). In IPITT, both young and aged *ob/ob* mice were severely insulin resistant, with young mice showing paradoxically elevated blood glucose after insulin injection, as reported previously [32] (Supplementary Figure 5D). The large variations in insulin sensitivity in aged *ob/ob* mice may reflect the variations in body weight (Supplementary Figure 5A and D). Aged *ob/ob* mice exhibited reduced insulin content as well as a leftward shift of glucose sensitivity with a half-maximal response at about 2.8 mM, well below that of normal mice (10−12 mM) [33] (Supplementary Figure 5E and F).

These results demonstrate that aged β cells share the following characteristics: hypersensitivity to glucose and reduced insulin content. However, these phenotypes were not homogeneous but depended partly on the strain. Hypersensitivity to glucose was most pronounced in aged *ob/ob* mice, indicating that obesity promotes age-associated β-cell hyperfunction.

3.2. Glycolysis is increased in aged islets

To determine whether alterations in glucose metabolism underlie hypersensitivity to glucose in aged islets, we performed [U-^{13}C] glucose tracing. Islets were stimulated for 1 h with 2.8 mM (2.8G) or 11.1 mM (11G) glucose isotopomer [U-^{13}C]-glucose, in which all of the six carbon atoms are replaced with ^{13}C. ^{13}C is incorporated into the intermediates of glucose metabolism (Figure 2A), which were quantified by capillary electrophoresis/time-of-flight mass spectrometry (CE/TOFMS). Metabolic flux was assessed by the enrichment (%) of ^{13}C in all carbon atoms of each metabolite, as described previously [27].

Islets from aged R1 showed higher ^{13}C enrichment than islets from young R1 in most glycolysis intermediates (G6P-3PG) and TCA intermediates (citrate and malate) (Figure 2B, Supplementary Figure 8A). Similarly, young P1 islets showed higher ^{13}C enrichment than young R1 in glycolysis intermediates, which was further increased in aged P1. We also found a trend toward a higher ATP/ADP ratio (Figure 2B), suggesting that increased glycolytic flux underlies enhanced glucose sensitivity in aged islets. Of note, no age-dependent increase in ^{13}C enrichment was observed for acetyl CoA, indicating that aging enhances carbon flux from glycolysis to the TCA cycle mainly through an anaplerotic pathway that bypasses acetyl CoA (Figure 2A) [34], as seen in juvenile and adult B6 β cells [27].

We further examined the glucose metabolic flux in B6 and *ob/ob* islets. Aged B6 islets showed increased ^{13}C enrichment in the intermediates of later glycolytic steps (2PG-lactate), mainly at 11G (Supplementary Figure 6). Upregulation of glycolysis was more pronounced in aged *ob/ob* islets, which showed increased ^{13}C enrichment in most glycolysis intermediates at both 2.8G and 11G (Supplementary Figure 7). Collectively, these results demonstrate that hypersensitivity to glucose in aged β cells reflects the upregulation of glycolysis.

Although aged B6 islets displayed slightly increased ^{13}C enrichment in acetyl CoA, the increment was less than the related metabolites (pyruvate and malate) and was absent in aged *ob/ob* islets (Supplementary Figures 6 and 7), indicating that the increased glycolytic flux enters the mitochondria mainly through the anaplerotic pathway.

3.3. Cytosolic NAD metabolism is altered in aged islets

We then explored how glycolysis is increased in aged β cells. The first late-limiting step of glycolysis is controlled by hexokinases, which produce glucose 6-phosphate (G6P) [35]. ^{13}C enrichment in G6P was substantially increased in aged SAM islets, suggesting that the acceleration of this step contributes to the increased carbon flux in downstream glycolytic reactions (Figure 2B). By performing RT-qPCR, we found an increased expression of hexokinase 1 (*Hk1*) and hexokinase 2 (*Hk2*) (Figure 2C, Supplementary Table 1). Induction of these high-affinity hexokinases is expected to increase the sensitivity to glucose in β cells [36], possibly in compensation for the decreased expression of low-affinity glucokinase (*Gck*, also known as hexokinase 4) in aged SAM islets (Figure 2C, Supplementary Table 1).

For a more comprehensive transcriptional analysis, we performed RNA sequencing (RNA-seq) of young and aged B6 mouse islets. A cyclin-dependent kinase inhibitor *Cdkn2a* (encoding p16), an aged β-cell marker, was significantly increased in aged islets, consistent with the previous reports (Supplementary Table 2) [9,10]. We then examined the genes involved in glucose metabolism as defined by Gene Ontology terms (Supplementary Table 2). Among the 69 genes significantly regulated by aging, the largest fold change was found in *Nmnat2*, a cytosolic enzyme that synthesizes NAD from nicotinamide mononucleotide (NMN) and ATP (Figure 2A). Since glycolysis requires NAD for the oxidation of GA3P (Figure 2A), we hypothesized that upregulated *Nmnat2* activates glucose metabolism by supplying cytosolic NAD in aged β cells, as reported in adipocyte differentiation [28]. In fact, *Nmnat2* was increased with aging in islets of all of the strains examined (R1, P1, *ob/ob*, and B6) (Figure 2D, Supplementary Figure 8C). In line with our hypothesis, intracellular NAD was increased with aging in both R1 and P1 (Figure 2B). Co-immunostaining for Nmnat2 and insulin revealed that Nmnat2 is predominantly localized to β-cell cytosol and is increased with aging (Figure 2E).

In addition to Nmnat2, oxidation of NADH contributes to the maintenance of cytosolic NAD by modulating the NAD/NADH ratio, a process carried out by three pathways: the glycerol phosphate (GP) shuttle, the malate-aspartate (MA) shuttle, and lactate production (Figure 2A). ^{13}C enrichment in glycerol 3-phosphate (G3P) and lactate tended to increase with aging in both strains (Figure 2B), indicating that these pathways are activated in relation to increased glycolytic flux. In contrast, ^{13}C enrichment in Asp and Glu at 11G, a marker of MA shuttle activity [25], failed to show any apparent increase in aged R1 compared with young R1 (Figure 2B). Using older (98-week) R1 islets, we further confirmed that ^{13}C enrichment in Asp and Glu was reduced with aging (Supplementary Figure 8B). Supporting these findings, aged R1 islets showed decreased MA shuttle enzymes (*Got1* and *Mdh1*) along with increased *Ldha* compared with young R1 islets (Figure 2C, Supplementary Table 1). Young P1 islets also trended toward increased lactate production and decreased MA shuttle activity compared with young R1 islets (Figure 2B and C, Supplementary Table 1). We observed no significant decline in the MA shuttle activity in aged P1 islets compared with young P1 islets (Figure 2B). The NAD/NADH ratio showed no age-associated change in either R1 or P1 (Figure 2B), indicating that the decline in the MA shuttle activity is
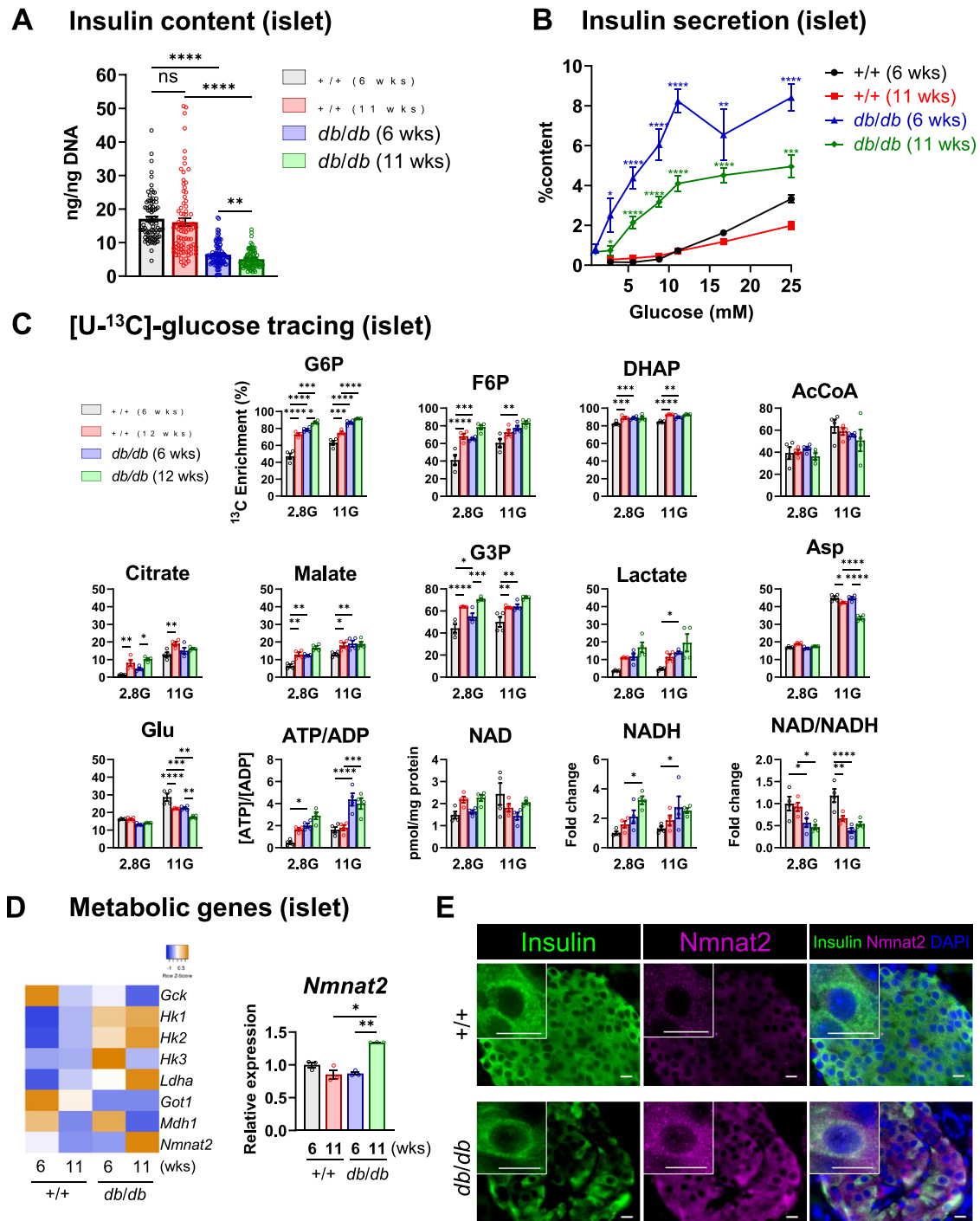
Figure 3: Diabetic islets show altered function and metabolism similar to aged islets. (A) Insulin content in islets normalized to the DNA content. +/+ (6 wks): n = 85; +/+ (12 wks): n = 85; db/db (6 wks): n = 102; db/db (12 wks): n = 87. Statistical comparisons were made by one-way ANOVA with Dunnett's post hoc test between the indicated pairs. (B) Dose-dependent effects of glucose on insulin secretion from +/+ and db/db islets. n = 10−16 for each. Asterisks indicate significant differences from age-matched +/+ by Welch's unpaired t-test. (C) [U-^{13}C]-glucose tracing experiment in +/+ and db/db islets. Enrichment of ^{13}C for the indicated metabolites following a 1-h incubation with 2.8 mM (2.8G) or 11.1 mM [U-^{13}C]-glucose (11G) were measured. For NAD and NADH, the intracellular content is indicated. n = 4 for each. Statistical comparisons were made by two-way ANOVA with Tukey's post hoc test. See also Supplementary Figure 9E for other metabolites. (D) Left, expression of metabolic genes in +/+ and db/db islets at 6 and 11 weeks of age assessed by RT-qPCR. n = 3 for each. Right, the relative expression of Nmnat2. Statistical analysis was performed by one-way ANOVA with Dunnett's post hoc test between the following comparisons: +/+ (6 wks) vs. +/+ (11 wks), +/+ (6 wks) vs. db/db (6 wks), db/db (6 wks) vs. db/db (11 wks), and +/+ (11 wks) vs. db/db (11 wks). Means of each group are visualized. The heatmap scale is Z score for the number of deviations away from the row mean. See Supplementary Table 3 for quantitative values. (E) Immunofluorescence staining of the pancreatic sections from +/+ (25 wks) and db/db (25 wks) for Insulin (green) and Nmnat2 (magenta). Nuclei were stained with DAPI (blue). Scale bars, 10 μm. Insets show the representative cells. Data are represented as mean ± SEM for (A)−(D). **p < 0.01, ***p < 0.001, ****p < 0.0001, ns, not significant.

compensated for by the activation of the other two cytosolic NADH oxidation pathways.

To summarize the age-associated metabolic alterations in β cells, transcriptional changes of *Gck*, *Hk1*, *Hk2*, and *Nmnat2* may contribute to increased glycolytic flux, providing glycolytic intermediates for the GP shuttle and lactate production, compensating for the decreased MA shuttle activity.

3.4. Diabetic islets show altered function and metabolism similar to aged islets

The aging models in the present study (SAM, B6, or *ob/ob*) did not develop diabetes spontaneously. However, under metabolic stress such as obesity and insulin resistance, glucose hyperresponsiveness as well as increased glucose metabolism in β cells are thought to represent compensatory hyperfunction, which finally results in β-cell dysfunction [3,37]. We therefore sought to clarify the relationship between the age-associated β-cell metabolic changes and β-cell dysfunction using *db/db* mice (BKS.Cg-+*Lepr*^{db}/+*Lepr*^{db}) as a model of obesity-related T2D and +/+ mice (BKS.Cg-*m*+/*m*+) as lean controls.

Body weight and ad libitum-fed blood glucose levels in 6-week-old *db/db* mice were already higher than those in age-matched +/+ mice, and increased steadily until 12 weeks (Supplementary Figure 9A). In the fasting state, 6-week-old *db/db* mice exhibited elevated glucose and plasma insulin compared with age-matched +/+ mice (Supplementary Figure 9B and D). In OGTT, 6-week-old *db/db* mice showed impaired glucose tolerance and higher plasma insulin levels compared with age-matched +/+ mice (Supplementary Figure 9C and D). These findings were further evident in 11-week-old *db/db* mice (Supplementary Figure 9C and D). Consistently with these systemic changes, 6-week-old *db/db* islets showed enhanced glucose responsiveness despite the reduced insulin content compared with age-matched +/+ islets (Figure 3A and B). 11-week-old *db/db* islets showed a decline in both glucose responsiveness and insulin content compared with age-matched +/+ islets and 6-week-old *db/db* islets (Figure 3A and B). These results indicate that 6-week-old *db/db* mice are already diabetic and that β-cell failure in 11-week-old *db/db* mice further exacerbates glucose intolerance.

In [U-¹³C] glucose tracing, 6- and 12-week-old *db/db* islets showed or tended to show increased ¹³C enrichment in glycolysis intermediates and TCA intermediates, with a parallel increase in ATP/ADP ratios compared with age-matched +/+ islets (Figure 3C). 12-week-old *db/db* islets tended to show even higher ¹³C enrichment in most intermediates than 6-week-old *db/db* islets, indicating that diabetes progression leads to further upregulation of glucose metabolism (Figure 3C). *db/db* islets also showed increased ¹³C enrichment in G3P and lactate, similar to most other intermediates, while opposite changes were found in Asp and Glu at 11G. Consistent with these metabolic changes, *db/db* islets showed or tended to show increased *Hk1*, *Hk2*, and *Ldha* along with decreased *Gck* and *Got1* compared with age-matched +/+ islets (Figure 3D left, Supplementary Table 3). Unlike aged mouse islets, there was an increase in NADH without changes in NAD in *db/db* islets, leading to a lowered NAD/NADH ratio compared with +/+ islets (Figure 3C). This finding suggests that the decline in the MA shuttle is not fully compensated. This may be due to insufficient induction of *Nmnat2*, which was increased only in 11-week-old *db/db* islets compared with 6-week-old *db/db* or age-matched +/+ islets, with a smaller change (~1.5 fold, Figure 3D right) than in aging SAM islets (more than 2.5 fold, Figure 2D). Nevertheless, we confirmed increased Nmnat2 immunoreactivity in the β cells of 25-week-old *db/db* islets compared with that in age-matched +/+ islets (Figure 3E). Increased glucose responsiveness, glycolysis, and altered expression of

metabolic genes were observed not only in *db/db* islets but also in the comparison between 6-week-old and 11—12-week-old +/+ islets (Figure 3B—D). As +/+ and *db/db* share the BKS genomic background, our results suggest that these metabolic changes are associated with the BKS genome. In fact, the BKS genome partly derived from DBA/2 mice, a strain characterized by susceptibility to β-cell failure [38,39]. DBA/2 islets exhibit hyperactive glycolysis compared with B6 [40]. Collectively, these results demonstrate that (1) diabetic islets are characterized by hypersensitivity to glucose, increased glycolysis, altered cytosolic NAD metabolism, and reduced insulin content, similarly to aged islets and (2) glucose responsiveness declines with the progress of diabetes even though glycolysis is further increased, which is consistent with developing β-cell failure [3,41].

3.5. β-Cell identity is similarly compromised in aging and diabetes

A loss of β-cell identity is defined as the failure to express the full complement of β-cell genes or expression of genes not normally expressed in mature, healthy β cells [41]. Because compromised β-cell identity has been observed in diabetic β cells and is associated with β-cell dysfunction [3,41,42], we investigated whether dysfunctional phenotypes in aged SAM and *db/db* islets are related to the loss of β-cell identity. Most of the β-cell-enriched genes including transcription factors (*Mafa*, *Foxo1*, *Nkx6-1*, *Pdx1*) [43] and other functionally important genes (*Ins1*, *Ins2*, *Slc2a2* [encoding Glut2], *Slc30a8* [encoding ZnT8]) [42] were already lower in 6-week-old *db/db* islets than in age-matched +/+ islets and were further downregulated in 11-week-old *db/db* islets (Figure 4A, Supplementary Table 3). *Sox9* and *Aldh1a3*, markers of β-cell dedifferentiation [44,45] were consistently higher in *db/db* islets than in +/+ islets. Similarly, most of the β-cell-enriched genes were already lower in young P1 islets than in young R1 islets. They were also downregulated in aged R1 islets (Figure 4B, Supplementary Table 1). *Sox9* and *Aldh1a3* showed opposite changes. We next sought to confirm the loss of β-cell identity by immunohistochemistry. We first examined the expression of MafA, Nkx-6.1, and Pdx1 by co-staining with insulin; these transcription factors were reported to be an indicator of β-cell dysfunction in diabetes, showing reduced expression and altered subcellular localization [46]. MafA was expressed in the nucleus of +/+ β cells, whereas it was diffusely localized to the cytoplasm in *db/db* β cells, as reported previously in diabetic mice and humans (Figure 4C) [46,47]. The same phenomenon was observed in the β cells of aged R1 and aged P1 compared with young mice (Figure 4C). Nkx-6.1 showed cytosolic localization similar to MafA in *db/db* β cells (Supplementary Figure 10A), consistent with previous reports [47]. Similarly, Nkx-6.1 showed increased cytosolic distribution in the β cells of young P1, aged R1, and aged P1 compared with young R1 (Supplementary Figure 10B). Pdx1 immunoreactivity was decreased in *db/db* β cells compared with +/+ cells (Supplementary Figure 11A), although no apparent difference was observed in young or aged R1 and P1 (Supplementary Figure 11B). We also found increased Aldh1a3 immunoreactivity in *db/db* β cells compared with that in +/+ cells, as well as in the β cells of young P1, aged R1, and aged P1 compared with young R1 (Figure 4D), which is consistent with gene expression data (Supplementary Tables 1 and 3). These transcriptional and immunohistochemical analyses demonstrate that β-cell identity is similarly impaired in aging and diabetes.

Furthermore, we observed co-localization of Nmnat2 and Aldh1a3 immunoreactivity in *db/db* islets (Figure 4E, white arrows). Cells with relatively high Nmnat2 immunoreactivity also tended to lack nuclear Nkx-6.1 expression (Figure 4F, dashed rectangles). These findings suggest that β cells with higher Nmnat2 expression are more prone to lose their identity.
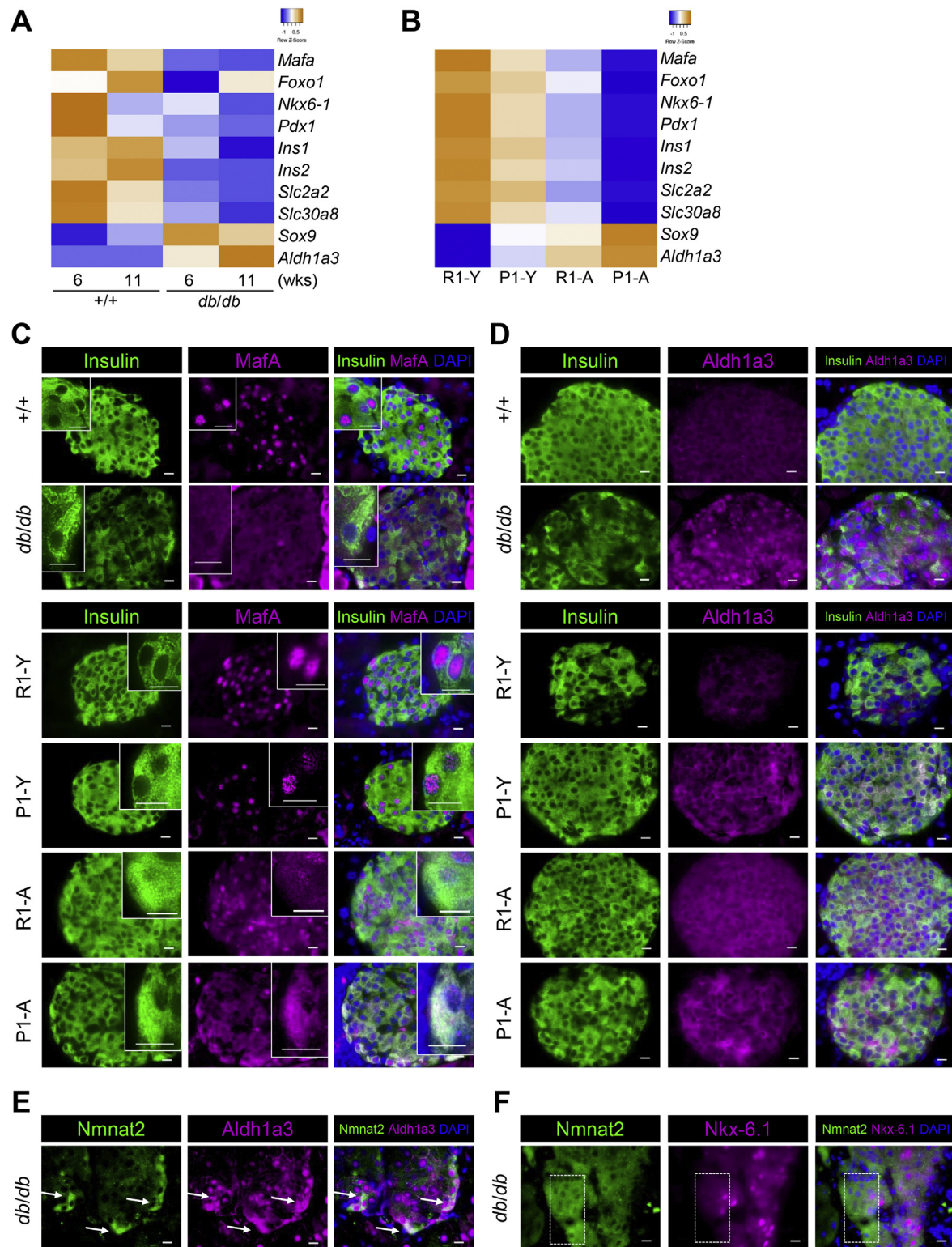
Figure 4: Altered expression of β-cell identity genes in aged and diabetic islets. (A)−(B): Expression of β-cell identity genes in islets assessed by RT-qPCR. Means of each group are visualized. Heatmap scales represent the Z score for the number of deviations away from the row mean. (A) +/+ and *db/db* islets at 6 and 11 weeks of age. n = 3 for each. See Supplementary Table 3 for quantitative values. (B) R1-Y: 27 wks, n = 4; P1-Y: 27 wks, n = 4; R1-A: 97 wks, n = 3; P1-A: 50 wks, n = 3. See Supplementary Table 1 for quantitative values. (C)−(F): Immunofluorescence staining of the pancreatic sections. +/+: 25 wks; *db/db*: 25 wks; R1-Y: 16 wks; P1-Y: 16 wks; R1-A: 84 wks; P1-A: 84 wks. Nuclei were stained with DAPI (blue). Scale bars, 10 μm. Insets show the representative cells. (C) Insulin (green) and MafA (magenta). (D) Insulin (green) and Aldh1a3 (magenta). (E) Nmnat2 (green) and Aldh1a3 (magenta). White arrows indicate the co-localization of Nmnat2 and Ald1a3 immunoreactivity. (F) Nmnat2 (green) and Nkx-6.1 (magenta). Dashed rectangles indicate the areas of relatively high Nmnat2 immunoreactivity.

3.6. *Got1* deletion accelerates glycolysis and impairs β-cell function and identity

The molecular mechanism accounting for the commonalities between the β-cell phenotypes in aging and diabetes is unknown. To test whether hyperactive glycolysis underlies these phenotypes, we turned to β cell lines deficient in glutamate-oxaloacetate transaminase 1 (*Got1* KO β cells). *Got1* is a component of the MA shuttle that transfers amino residue from Asp to α-ketoglutarate, generating glutamate and oxaloacetate. We expected that *Got1* deletion would increase the glycolytic flux as reported in cancer cells [48] and thereby recapitulate hyperactive glycolysis in aged β cells.

We previously established two independent *Got1* KO β cell lines (*Got1* KO-1 and -2) [25] from mouse clonal β-cell MIN6-K8 (hereafter referred to as parental cells) [24]. As expected, in [U-^{13}C]-glucose tracing, *Got1* KO β cells showed increased ^{13}C enrichment compared with parental cells in all examined glycolysis intermediates, citrate, G3P, and lactate (Figure 5A, Supplementary Figure 12A). Changes in metabolic gene expression were observed similarly to aged and diabetic islets (Figure 5B, Supplementary Table 4). *Got1* KO β cells displayed decreased ^{13}C enrichment in Asp at 11G, indicating defective MA shuttle activity. However, different from aged or diabetic islets, ^{13}C enrichment in Asp and Glu at 2.8G were higher in *Got1* KO β cells. *Got1* KO-1 also showed higher ^{13}C enrichment in Glu at 11G (Figure 5A). These paradoxical findings suggest compensatory activation of biosynthetic pathways that bypass Got1. ^{13}C flux to the TCA cycle is substantially increased by *Got1* deletion at 2.8G (Figure 5A). Under this condition, Asp and Glu are likely to be predominantly synthesized from TCA intermediates by mitochondrial isozyme Got2 and glutamate dehydrogenase (encoded by *Glud1*), respectively.

Inactivation of the MA shuttle was also indicated by increased NADH as well as a decreased NAD/NADH ratio in *Got1* KO β cells compared with parental cells (Figure 5A), as reported previously in *Got1*-deficient cancer cells [48,49]. We confirmed the induction of Nmnat2 by RT-PCR and immunocytochemistry (Figure 5C). It is noteworthy that *Got1* KO β cells showed comparable NAD levels to parental cells (Figure 5A), unlike previously reported *Got1*-deficient cancer cells that show decreased NAD levels [48,49]. This finding supports our hypothesis that β cells compensate for the decrease in NADH re-oxidation by increasing Nmnat2-mediated NAD synthesis. Collectively, metabolic tracing and gene expression analyses revealed that genetic ablation of *Got1* phenocopies age-associated metabolic alterations in β cells.

Got1 KO β cells showed reduced insulin content (Figure 5D), hypersensitivity to glucose (Figure 5E), and loss of identity (Figure 5F, Supplementary Table 4) compared with parental cells. These results demonstrate that metabolic alterations by *Got1* deletion dysregulate β-cell function and identity similarly to that seen in aging and diabetes. The phenotypes of *Got1* KO-1 and KO-2 were consistent, albeit with minor differences. *Got1* KO-1 displayed slightly more active glycolysis than KO-2 likely due to the higher expression of *Hk1*, *Hk2*, *Ldha*, and *Nmnat2* (Figure 5A and B, Supplementary Figure 12A). However, the reduction in insulin content was less substantial in *Got1* KO-1 than in KO-2. These differences may be due to the heterogeneity exhibited by MIN6 sub-clones with increasing passage numbers [50,51]. We selected *Got1* KO-1 as a model of hyperactive glycolysis for further analysis.

3.7. Attenuation of glycolysis restores β-cell identity and function

To clearly establish a causal role of hyperactive glycolysis in the loss of β-cell identity, we tested whether impaired identity in *Got1* KO-1 can be restored by attenuating glycolysis. To chronically restrict glucose uptake, the cells were cultured for 4 days in the presence of low

glucose (LG) or 2DG, a glucose analog that blocks glycolysis. LG concentrations were 5 and 0.05 mM for parental and *Got1* KO-1, respectively, approximating the Km of the predominant hexokinase isotype, Gck (Km = 8 mM), in parental cells and Hk1/2 (Km = 0.01−0.05 mM) in *Got1* KO-1 [36]. Transcription factors specific to mature β cells (*Mafa*, *Foxo1*, *Nkx6-1*, *Pdx1*, and *Pax4*) and other β-cell-specific genes (*Slc2a2*, *Gck*, and *Glp1r*) were restored, while dedifferentiation markers (*Sox9* and *Aldh1a3*) as well as α-cell markers (*Mafb* and *Gcg*) were downregulated by either or both LG and 2DG (Figure 6A, Supplementary Table 5). Moreover, the increase in expression of *Ldha* and *Nmnat2* in *Got1* KO-1 was restored by either or both LG and 2DG, indicating that altered cytosolic NAD metabolism is an adaptive response to increased glycolytic flux (Figure 6A, Supplementary Table 5). LG and 2DG showed a marginal effect in parental cells. These results demonstrate that hyperactive glycolysis impairs β-cell identity.

To test our hypothesis that Nmnat2 mediates the impairment of β-cell function and identity by supplying NAD to activate glycolysis, we next knocked down *Nmnat2* by shRNA in parental and *Got1* KO-1, albeit with moderate efficiency in parental cells likely due to the low expression (Supplementary Table 6). We first confirmed that NAD, the ATP/ADP ratio, and ^{13}C enrichment in glycolysis and TCA intermediates were all decreased by *Nmnat2* knockdown in *Got1* KO-1 (Figure 6B). In contrast, glycolysis intermediates before the NAD-consuming step (G6P-G3P) were unaffected (Supplementary Figure 12B). These results demonstrate that Nmnat2 activates glycolysis by supplying NAD.

In *Got1* KO-1, *Nmnat2* knockdown restored the expression of transcription factors (*Mafa*, *Foxo1*, *Nkx6-1*, *Pdx1* and *Pax4*) and most other β-cell-specific genes (*Ins1*, *Ins2*, *Slc30a8*, *Slc2a2*, *Glp1r*) (Figure 6C, Supplementary Table 6). The restoration of β-cell-specific genes by *Nmnat2* knockdown was similar to that by the restriction of glucose uptake, and was more substantial for *Foxo1*, *Nkx6-1*, *Ins1*, and *Ins2*. Moreover, the insulin content was more than doubled, while sensitivity to glucose was decreased by *Nmnat2* knockdown in *Got1* KO-1 (Figure 6D and E). In contrast, *Nmnat2* knockdown showed little effect on any of the phenotypes in parental cells (Figure 6C−E).

To understand the mechanism by which Nmnat2 modulates various β-cell phenotypes, we examined whether Nmnat2 regulates NAD-dependent signaling pathways. Sirtuins (SIRTs) and poly (ADP-ribose) polymerases (PARPs) are key regulators of various cellular functions that consume NAD as a substrate [52]. We therefore tested whether Nmnat2 knockdown affects the activity of Sirt1 and Parp1. Because p53 is deacetylated by Sirt1 at lysine 379 [53], the activity of Sirt1 was assessed by monitoring acetyl-p53 (Ac-p53 K379), as shown in previous reports [28]. *Nmnat2* knockdown decreased Ac-p53 (K379) in *Got1* KO-1, indicating the increased activity of Sirt1 (Figure 6F). Similarly, *Nmnat2* knockdown increased the poly (ADP-ribose) (PAR) levels in *Got1* KO-1, indicating the increased activity of Parp1. In contrast, *Nmnat2* knockdown showed no significant effect in parental cells (Figure 6F). These results indicate that the upregulation of Nmnat2 decreases the activities of Sirt1 and Parp1, as previously reported in adipocyte differentiation [28].

Collectively, our data suggest that (1) Nmnat2 hardly plays any role in normal β cells but (2) Nmnat2 is upregulated in aged or diabetic β cells, activating glycolysis and supressing the activities of Sirt1 and Parp1, adversely affecting β-cell function and identity.

4. DISCUSSION

In the present study, we have shown that (1) β cells become dysfunctional and lose identity with aging; (2) hyperactive glycolysis
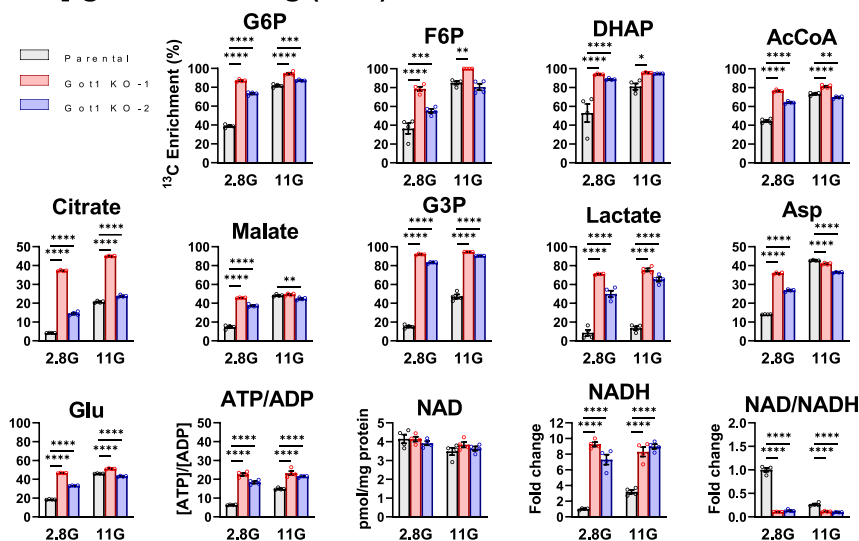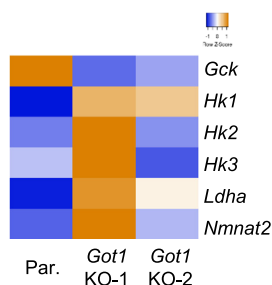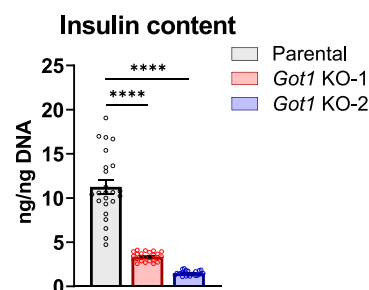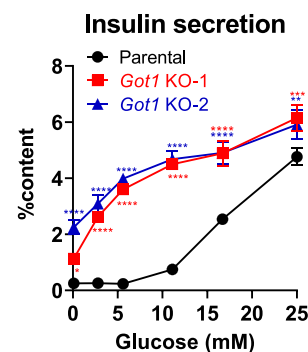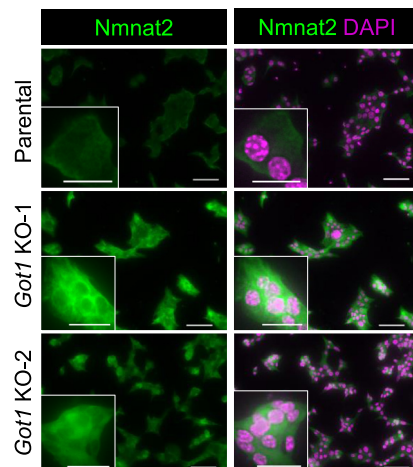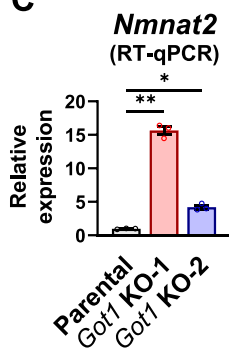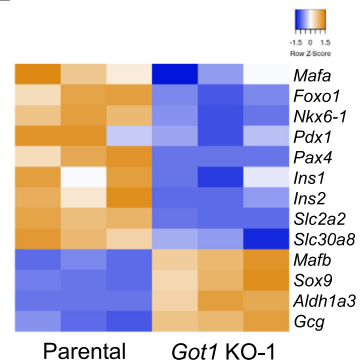
Figure 5: Metabolic alteration by *Got1* deletion dysregulates β-cell function and identity. (A) [U-^{13}C]-glucose tracing experiment in parental cells and two independent *Got1* KO β cells (*Got1* KO-1 and -2). Enrichment of ^{13}C for the indicated metabolites following a 30-min incubation with 2.8 mM (2.8G) or 11.1 mM [U-^{13}C]-glucose (11G) were measured. For NAD and NADH, the intracellular content is indicated. n = 4 for each. Statistical comparisons were made by two-way ANOVA with Tukey's post hoc test. See also Supplementary Figure 12A for other metabolites. (B) Expression of metabolic genes in parental and *Got1* KO β cells determined by RT-qPCR. n = 3 for each. Means of each group are visualized. See Supplementary Table 4 for quantitative values. (C) Left, the relative expression of *Nmnat2*. See the legend of Figure 5B for the experimental details. Statistical comparisons were made by one-way ANOVA with Dunnett's post hoc test between the parental cells and *Got1* KO-1 or KO-2. Right, immunostaining of parental and *Got1* KO β cells for Nmnat2 (green). Nuclei were stained with DAPI (magenta). Scale bars, 50 μm. Insets show the representative cells (scale bars, 20 μm). (D) Insulin content normalized by the DNA content. n = 24. Statistical comparisons were made by one-way ANOVA with Dunnett's post hoc test between the parental cells and *Got1* KO-1 or KO-2. (E) Dose-dependent effects of glucose on insulin secretion from parental and *Got1* KO β cells. Asterisks indicate the statistical differences from parental cells. n = 4. Statistical comparisons were made by two-way ANOVA with Dunnett's post hoc test between parental cells and *Got1* KO-1 or KO-2. (F) Expression of β-cell identity genes in parental and *Got1* KO-1 determined by RT-qPCR. n = 3 for each. Individual values are visualized. See Supplementary Table 4 for quantitative values. Data are represented as mean ± SEM for (A), (C), (D), and (E). *p < 0.05, **p < 0.01, ***p < 0.001, ****p < 0.0001. Heatmap scales represent the Z score for the number of deviations away from the row mean.

may cause the dysfunction and compromised identity of aged and diabetic β cells; and (3) Nmnat2, an NAD-synthesizing enzyme, may be the functional link between hyperactive glycolysis and dysregulation of β cells.

Previous studies have highlighted the potential benefits of age-associated enhancement in GIIS to maintain glucose homeostasis. However, our analyses reveal phenotypic similarities between aged and diabetic β cells including hypersensitivity to glucose, reduced insulin content, and compromised identity, demonstrating that β-cell function and identity are impaired with aging. Previous studies have reported β-cell dysfunction and impaired identity under hyperglycemia, which are consistent with our observations in *db/db* mice. However, our results from aged mice demonstrate that β cells can become defective even without preceding hyperglycemia. We therefore propose that hyperactive glycolysis is a common metabolic trait in aged and diabetic β cells and it underlies age-associated β-cell dysfunction and loss of identity.

Hyperactive glucose metabolism has been observed in β cells of various obese and diabetic rodent models. For example, increased glucose utilization has been found in these β cells and ascribed to the increased expression of low-affinity hexokinases [54—57], consistent with our results in aged SAM, *db/db* mice, and *Got1* KO cells. Decreased *Gck* expression negatively affects glucose sensitivity as observed in β cells of *db/db* mice with *Gck* haploinsufficiency [58]. However, since Hk exhibit substantially more glucose utilization than Gck at low (3 mM) and high (20 mM) glucose [36], increased *Hk* expression may well compensate for decreased *Gck* in aged and diabetic β cells. Previous reports also show the enhancement of anaplerosis via pyruvate carboxylase [59] and increased mitochondrial activity [60,61], supporting our metabolic and transcriptional characterization of aged and diabetic islets (Figures 2B, C and 3C, D).

Compromised β-cell identity has also been observed in various diabetic rodent models [44,62—64] as well as diabetic human subjects [47,65,66]. Several mechanisms have been proposed for the loss of β-cell identity, including a loss of transcription factor FoxO1 [44,67], maladaptive unfolded protein response (UPR) under endoplasmic reticulum (ER) stress [42], inflammation [68], and oxidative stress [46]. It is likely that hyperactive glycolysis is involved in these pathways. For example, excess glycolytic intermediates trigger ER stress [69] and oxidative stress [70]. Furthermore, loss of β-cell identity leads to increased glycolysis by disrupting key β-cell metabolic genes including *Slc2a2*, *Gck*, *Hk1*, *Hk2*, and *Ldha* [42,71]. Recent evidence demonstrates that FoxO1 suppresses glycolytic genes and thereby protects β cells from excess glycolysis and dysfunction [72—74]. These studies further support the hypothesis that attenuation of hyperactive glycolysis prevents the impairment of β-cell function and identity.

Our study identifies Nmnat2 as a novel metabolic regulator in β cells. Nmnat1-3 synthesizes NAD from NMN and ATP in distinct and mutually exclusive subcellular compartments [75,76]. Nmnat2 localizes to the cytoplasm and Golgi and regulates cytosolic NAD levels [77]. Previous studies on Nmnat2 mostly focused on its role as a neuronal survival factor [78]. NMNAT2 is also expressed in human islets [79], but its function in islet cells has not been established. In normal β cells, at physiological glucose concentrations, the combined activities of the MA and GP shuttles are sufficient to allow stoichiometric re-oxidation of cytosolic NADH to maintain glycolysis [80,81]. With aging or diabetes, the MA shuttle declines while the glycolytic flux is increased (Figures 2B, C and 3C, 3D). When increased glycolytic flux exceeds the net activity of the two shuttles, we observed that NAD generated by lactate dehydrogenase and Nmnat2 contributes to the maintenance of the cytosolic NAD pool. In line with this hypothesis, *Nmnat2*, *Ldha*, and

^{13}C flux to lactate were concurrently increased in aged islets, diabetic islets, and *Got1* KO cells (Figures 2B, C, 3C, D, and 5A, B). Given that the induction of *Nmnat2* and *Ldha* depends on glucose utilization (Figure 6A, Supplementary Table 5), it is strongly suggested that alterations in cytosolic NAD metabolism parallel the increased glycolytic flux.

We have also shown that increased Nmnat2 negatively regulates the activities of Sirt1 and Parp1 in β cells (Figure 6F). Similar findings have been reported by Ryu et al. in adipocyte differentiation; since NMNAT2 and nuclear isozyme NMNAT1 compete for NMN, the upregulation of NMNAT2 leads to the depletion of nuclear NAD, which results in decreased activity of nuclear NAD-dependent enzymes [28].

Sirt1 plays an essential role in GIIS [82]. A loss of Sirt1 activity has been associated with the impairment of β-cell function with aging [83] and in diabetes [84]. In addition, it has been reported that Parp1 suppresses glycolysis by inhibiting Hk1 in neurons [85] and in cancer cells [86], suggesting that decreased Parp1 activity contributes to hyperactive glycolysis in β cells. Thus, our results indicate that Nmnat2-mediated crosstalk between glucose metabolism and intracellular signaling is involved in the impairment of β-cell function in aging and diabetes.

It is also noteworthy that *Nmnat2* expression and function is restricted to dysfunctional β cells; no significant phenotype was observed by *Nmnat2* knockdown in parental β cells (Figure 6C—F). As such, *Nmnat2* suppression is a promising therapeutic approach allowing for the selective modulation of dysfunctional β cells.

Although the present study identified the metabolic features shared in common among multiple mouse models of aging and diabetes, some of the findings may reflect strain differences.

First, glucose excursions were decreased in aged P1 compared with young P1 and aged R1, despite the lack of increase in plasma insulin levels or insulin sensitivity (Figure 1C and D, Supplementary Figure 1D—H). Because SAMP1 displays nephropathic changes [87], urinary glucose excretion may well be increased in aged P1. As the glucagon levels are reduced in SAMP6 [88], counter-regulatory hormones may also be involved.

Second, age-associated changes in insulin content were found to vary with strain; R1 showed no change with aging, while P1 displayed reduced insulin content from a young age, similarly to *db/db* mice (Figures 1E and 3A). An age-dependent decrease was observed in the other aging models (B6 and *ob/ob*) (Supplementary Figures 4E and 5E). These differences may be associated with oxidative stress. It has been reported that oxidative stress depletes insulin in diabetic β cells [89,90] and is increased in various organs with aging [91]. In fact, increased oxidative stress has been found in P1 from a young age [18,20,21], which is consistent with the low insulin content (Figure 1E). As R1 was interbred against the phenotypes of P1 [21], the mice may be genetically resistant to oxidative stress.

Third, although glycolysis was increased in aged P1 islets compared with young P1 islets, aged P1 islets showed no decline in *Got1* expression or MA shuttle activity (Figure 2B, Supplementary Table 1). In SAMP8, muscle cells increased their mitochondrial metabolism and glucose uptake to adapt to oxidative stress [92]. A similar mechanism may compensate for age-associated changes in NAD/NADH metabolism in aged P1.

Fourth, NAD metabolism was partially different between aging mice and *db/db* mice, with *db/db* mice showing less induction of *Nmnat2* compared with aged mice (Figures 2D and 3D, Supplementary Figure 8C) along with increased NADH (Figure 3C), as explained in section 3.4. Excess NADH may be attributable to several factors. Hyperglycemia-induced mitochondrial dysfunction may decrease
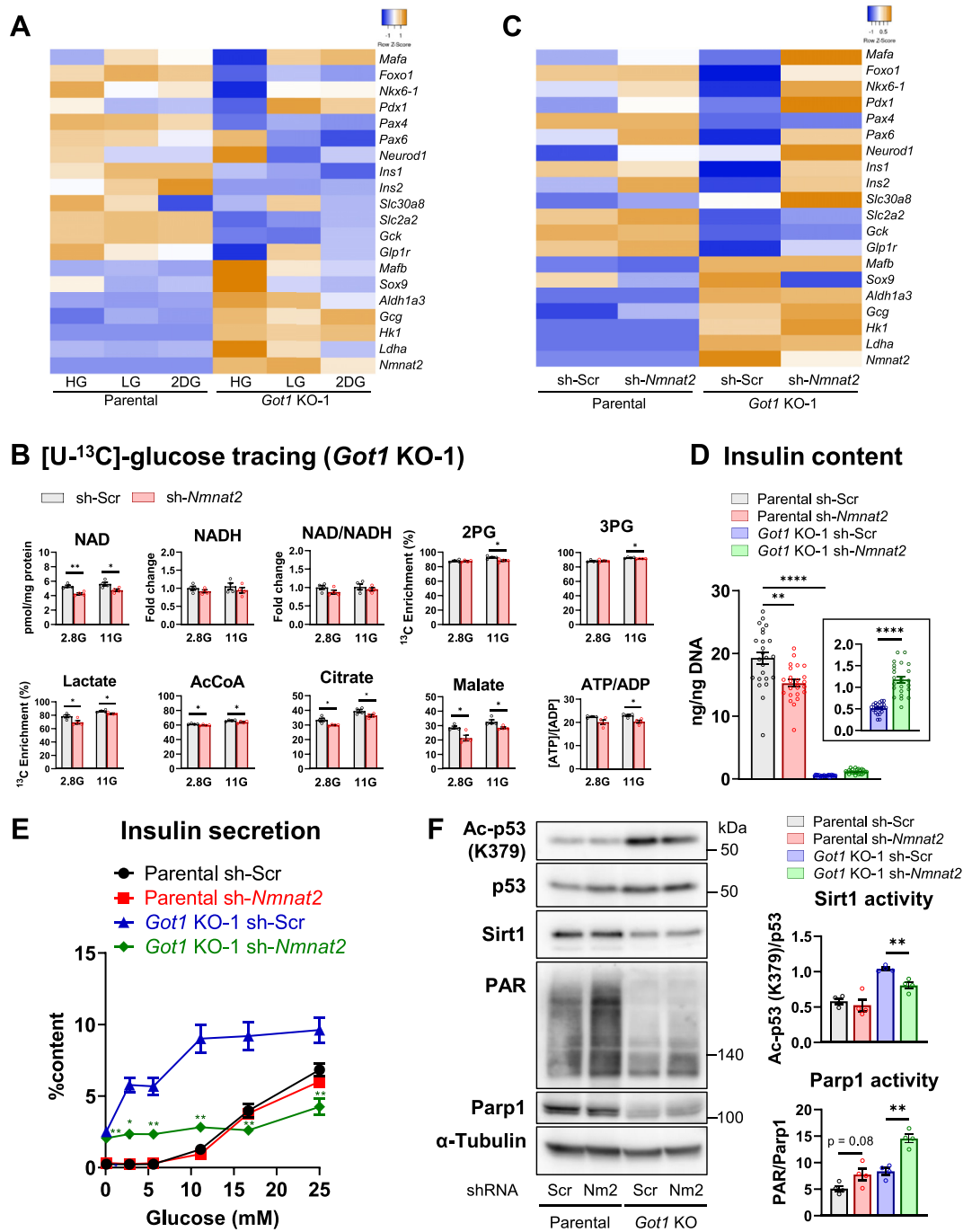
Figure 6: Suppression of *Nmnat2* improves β-Cell identity and function. (A) Effects of chronic treatment with high glucose (HG: 25 mM glucose), low glucose (LG: 5 mM for parental cells; 0.05 mM for *Got1* KO-1), or 2-deoxy-ᴅ-glucose (2DG: 25 mM 2-deoxyglucose added to 25G) on the expression of β-cell identity genes assessed by RT-qPCR. n = 3 for each. Means of each group are visualized. See Supplementary Table 5 for quantitative values. (B)−(F): Effects of adenoviral shRNA-mediated knockdown of *Nmnat2* on the function and identity of parental cells and *Got1* KO-1. sh-Scr, scramble shRNA; sh-*Nmnat2*, Nmnat2 shRNA. (B) [U-^{13}C]-glucose tracing experiment in *Got1* KO-1. Enrichment of ^{13}C for the indicated metabolites following 30-min incubation with 2.8 mM (2.8G) or 11.1 mM [U-^{13}C]-glucose (11G) were measured. For NAD and NADH, the intracellular content is indicated. n = 4 for each. See also Supplementary Figure 12B for other metabolites. (C) Expression of β-cell identity genes assessed by RT-qPCR. n = 3 for each. Means of each group are visualized. See Supplementary Table 6 for the quantitative values. (D) Insulin content normalized by the DNA content. n = 24 for each. Statistical comparisons were made by one-way ANOVA with Dunnett's post hoc test between the indicated pairs. (E) Dose-dependent effects of glucose on insulin secretion. n = 4 for each. Statistical comparisons were made by unpaired Welch's unpaired *t*-test between *Got1* KO-1 sh-Scr and *Got1* KO-1 sh-*Nmnat2*. (F) Activities of Sirt1 and Parp1 assessed by Western blotting. Left, representative blots are shown. Right, intensity of acetyl-p53 (K379) and poly ADP-ribose (PAR) were normalized to that of total p53 and Parp1, respectively. Scr, scramble; Nm2, *Nmnat2*. n = 4 for each. Statistical comparisons were made by Welch's unpaired *t*-test between sh-Scr and sh-*Nmnat2*. Data are represented as the mean ± SEM for (B), (D)−(F). *$p < 0.05$, **$p < 0.01$, ****$p < 0.0001$. p-value is indicated in (F). The heatmap scale represents the Z score for the number of deviations away from the row mean.

NADH re-oxidation in *db/db* mice, as reported previously in islets of βV59M, a nonobese diabetic mouse [93]. Moreover, *Nmnat2* expression is positively correlated with age (Figure 2D, Supplementary Figure 8C) and negatively correlated with adiposity and inflammation [94]. Because the *db/db* mice were young (6—12 weeks) and showed increased adiposity and inflammation [95], induction of *Nmnat2* might have been counteracted. To further clarify the link between aging and diabetes, the impact of strain-specific pathophysiological factors such as body composition and nutritional condition should be investigated in future studies.

The question is whether age-associated changes in mouse β cells can be extrapolated to humans. Assessment of β-cell function through clinical measurements (such as OGTT and clamp tests) is challenging and confounded by many factors in aging subjects [96]. Nonetheless, clinical measurements indicate that both basal and glucose-stimulated insulin secretion are reduced in elderly subjects as compared with that in young subjects after controlling for insulin sensitivity [5,97,98]. Recent studies on GIIS from islets of elderly subjects are controversial, since it was either diminished [8,99] or unchanged [6] compared with that from islets of young subjects.

Thus, enhanced insulin secretion in aged mice [6—9] may not be directly extrapolated to humans. However, there are reports of increased basal insulin secretion [99], as well as reduced expression of identity genes in aged human islets [7], suggesting that the age-associated changes observed in mouse β cells are relevant to humans. Metabolically, some reports find reduced mitochondrial activity in aged human islets as assessed by the ATP content [99] or NAD(P)H utilization [8]. However, glycolysis in aged human islets remains unexplored.

Hypersensitivity to glucose in aged β cells leads to improved glucose tolerance in aged mice (Figure 1B, Supplementary Figures 1E, 4B, and 5B). However, given the similarity between aged and diabetic β cells, it is possible that persistent β-cell hyperfunction leads to β-cell failure [3,100], as exemplified by the decline in GIIS in the 11-week-old *db/db* mice (Figure 3B). Thus, the key question to ask is whether hyperactive glycolysis determines age-associated β-cell dysfunction and promotes the development of T2D. From an experimental viewpoint, it will require longitudinal studies of rodent models that allow for the manipulation of β-cell glucose metabolism and are subsequently integrated with glucose metabolism studies on aged human β cells.

In summary, our study demonstrates that increased glycolysis is a metabolic commonality between aged and diabetic β cells and that increased glycolysis induces β-cell dysfunction and loss of cellular identity, which is restored by *Nmnat2* knockdown. Thus, increased β-cell glycolysis is a key metabolic signature as well as a potential therapeutic target in the pathophysiology of T2D.

AUTHOR CONTRIBUTIONS

Conceptualization: N.M. and S.S.; Methodology: N.M.; Investigation: N.M. and T.H.; Writing — Original Draft: N.M.; Writing — Review & Editing: N.M., N.Y., H.T., and Y.M.; Data Curation: N.Y.; Visualization: N.M.; Supervision: N.Y., H.T., Y.M., and S.S.; Funding Acquisition: H.T. and S.S.

ACKNOWLEDGMENTS

CONFLICT OF INTEREST

The authors declare no conflict of interest.

APPENDIX A. SUPPLEMENTARY DATA

Supplementary data to this article can be found online at https://doi.org/10.1016/j.molmet.2021.101414.

REFERENCES

[1] Henquin, J.C., 2009. Regulation of insulin secretion: a matter of phase control and amplitude modulation. Diabetologia 52(5):739—751. https://doi.org/10.1007/s00125-009-1314-y.

[2] Prentki, M., Matschinsky, F.M., Madiraju, S.M., 2013. Metabolic signaling in fuel-induced insulin secretion. Cell Metabolism 18(2):162—185. https://doi.org/10.1016/j.cmet.2013.05.018.

[3] Hudish, L.I., Reusch, J.E., Sussel, L., 2019. β Cell dysfunction during progression of metabolic syndrome to type 2 diabetes. The Journal of Clinical Investigation 129(10):4001—4008. https://doi.org/10.1172/JCI129188.

[4] Cho, N., Shaw, J., Karuranga, S., Huang, Y., Rocha Fernandes, J.D., Ohlrogge, A., et al., 2018. IDF Diabetes Atlas: Global estimates of diabetes prevalence for 2017 and projections for 2045. Diabetes Research and Clinical Practice 138:271—281. https://doi.org/10.1016/j.diabres.2018.02.023.

[5] Chang, A.M., Halter, J.B., 2003. Aging and insulin secretion. American Journal of Physiology-Endocrinology and Metabolism 284(1):E7—E12. https://doi.org/10.1152/ajpendo.00366.2002.

[6] Almaça, J., Molina, J., e Drigo, R.A., Abdulreda, M.H., Jeon, W.B., Berggren, P.-O., et al., 2014. Young capillary vessels rejuvenate aged pancreatic islets. Proceedings of the National Academy of Sciences of the United States of America 111(49):17612—17617. https://doi.org/10.1073/pnas.1414053111.

[7] Avrahami, D., Li, C., Zhang, J., Schug, J., Avrahami, R., Rao, S., et al., 2015. Aging-dependent demethylation of regulatory elements correlates with chromatin state and improved β cell function. Cell Metabolism 22(4):619—632. https://doi.org/10.1016/j.cmet.2015.07.025.

[8] Gregg, T., Poudel, C., Schmidt, B.A., Dhillon, R.S., Sdao, S.M., Truchan, N.A., et al., 2016. Pancreatic β-cells from mice offset age-associated mitochondrial deficiency with reduced KATP channel activity. Diabetes 65(9):2700—2710. https://doi.org/10.2337/db16-0432.

[9] Helman, A., Klochendler, A., Azazmeh, N., Gabai, Y., Horwitz, E., Anzi, S., et al., 2016. p16 Ink4a-induced senescence of pancreatic beta cells enhances insulin secretion. Nature Medicine 22(4):412—420. https://doi.org/10.1038/nm.4054.

[10] Aguayo-Mazzucato, C., van Haaren, M., Mruk, M., Lee Jr., T.B., Crawford, C., Hollister-Lock, J., et al., 2017. β cell aging markers have heterogeneous distribution and are induced by insulin resistance. Cell Metabolism 25(4):898—910. https://doi.org/10.1016/j.cmet.2017.03.015 e895.

[11] Takeda, T., Hosokawa, M., Takeshita, S., Irino, M., Higuchi, K., Matsushita, T., et al., 1981. A new murine model of accelerated senescence. Mechanisms of Ageing and Development 17(2):183–194. https://doi.org/10.1016/0047-6374(81)90084-1.

[12] Hosokawa, M., Kasai, R., Higuchi, K., Takeshita, S., Shimizu, K., Hamamoto, H., et al., 1984. Grading score system: a method for evaluation of the degree of senescence in senescence accelerated mouse (SAM). Mechanisms of Ageing and Development 26(1):91–102. https://doi.org/10.1016/0047-6374(84)90168-4.

[13] Mori, M., Higuchi, K., 2013. Genetic characteristics of SAM strains. In: Akiguchi, I., Higuchi, K., Hosokawa, M., Hosokawa, T., Nomura, Y. (Eds.), The senescence-accelerated mouse (SAM): achievements and future directions. Elsevier. p. 37–42.

[14] Han, J., Hosokawa, M., Umezawa, M., Yagi, H., Matsushita, T., Higuchi, K., et al., 1998. Age-related changes in blood pressure in the senescence-accelerated mouse (SAM): aged SAMP1 mice manifest hypertensive vascular disease. Laboratory Animal Science 48(3):256–263.

[15] Aoyama, Y., Kim, T.Y., Yoshimoto, T., Niimi, K., Takahashi, E., Itakura, C., 2013. Impaired motor function in senescence-accelerated mouse prone 1 (SAMP1). Brain Research 1515:48–54. https://doi.org/10.1016/j.brainres.2013.03.053.

[16] Yabuki, A., Suzuki, S., Matsumoto, M., Nishinakagawa, H., 2002. Life span and renal morphological characterization of the SAMP1//Ka mouse. Experimental Animals 51(1):75–81. https://doi.org/10.1538/expanim.51.75.

[17] Haramizu, S., Ota, N., Hase, T., Murase, T., 2011. Aging-associated changes in physical performance and energy metabolism in the senescence-accelerated mouse. The Journals of Gerontology Series A: Biomedical Sciences and Medical Sciences 66(6):646–655. https://doi.org/10.1093/gerona/glr037.

[18] Park, J.W., Choi, C.H., Kim, M.S., Chung, M.H., 1996. Oxidative status in senescence-accelerated mice. The Journals of Gerontology Series A: Biological Sciences and Medical Sciences 51(5):B337–B345. https://doi.org/10.1093/gerona/51A.5.B337.

[19] Yamashita, Y., Chiba, Y., Xia, C., Hirayoshi, K., Satoh, M., Saitoh, Y., et al., 2005. Different adaptive traits to cold exposure in young senescence-accelerated mice. Biogerontology 6(2):133–139. https://doi.org/10.1007/s10522-005-3499-x.

[20] Choi, J.Y., Kim, H.S., Kang, H.K., Lee, D.W., Choi, E.M., Chung, M.H., 1999. Thermolabile 8-hydroxyguanine DNA glycosylase with low activity in senescence-accelerated mice due to a single-base mutation. Free Radical Biology and Medicine 27(7–8):848–854. https://doi.org/10.1016/j.freeradbiomed.2017.10.012.

[21] Chiba, Y., Fujisawa-Tsukaguchi, H., Nishikawa, T., Hosokawa, M., 2013. Higher oxidative stress status and mitochondrial alterations as a possible mechanism for senescence acceleration. In: Akiguchi, I., Higuchi, K., Hosokawa, M., Hosokawa, T., Nomura, Y. (Eds.), The senescence-accelerated mouse (SAM): achievements and future directions. Elsevier. p. 373–83.

[22] Yan, J., Fujii, K., Yao, J., Kishida, H., Hosoe, K., Sawashita, J., et al., 2006. Reduced coenzyme Q10 sulementation decelerates senescence in SAMP1 mice. Experimental Gerontology 41(2):130–140. https://doi.org/10.1016/j.exger.2005.11.007.

[23] Shimizu, C., Wakita, Y., Inoue, T., Hiramitsu, M., Okada, M., Mitani, Y., et al., 2019. Effects of lifelong intake of lemon polyphenols on aging and intestinal microbiome in the senescence-accelerated mouse prone 1 (SAMP1). Scientific Reports 9(1):1–11. https://doi.org/10.1038/s41598-019-40253-x.

[24] Iwasaki, M., Minami, K., Shibasaki, T., Miki, T., Miyazaki, J., Seino, S., 2010. Establishment of new clonal pancreatic β-cell lines (MIN6-K) useful for study of incretin/cyclic adenosine monophosphate signalling. Journal of Diabetes Investigation 1(4):137–142. https://doi.org/10.1111/j.2040-1124.2010.00026.x.

[25] Murao, N., Yokoi, N., Honda, K., Han, G., Hayami, T., Gheni, G., et al., 2017. Essential roles of aspartate aminotransferase 1 and vesicular glutamate transporters in β-cell glutamate signaling for incretin-induced insulin secretion. PLoS One 12(11):e0187213. https://doi.org/10.1371/journal.pone.0187213.

[26] Oduori, O.S., Murao, N., Shimomura, K., Takahashi, H., Zhang, Q., Dou, H., et al., 2020. Gs/Gq signaling switch in β cells defines incretin effectiveness in diabetes. The Journal of Clinical Investigation 130(12):6639–6655. https://doi.org/10.1172/JCI140046.

[27] Wortham, M., Benthuysen, J.R., Wallace, M., Savas, J.N., Mulas, F., Divakaruni, A.S., et al., 2018. Integrated in vivo quantitative proteomics and nutrient tracing reveals age-related metabolic rewiring of pancreatic β cell function. Cell Reports 25(10):2904–2918. https://doi.org/10.1016/j.celrep.2018.11.031 e2908.

[28] Ryu, K.W., Nandu, T., Kim, J., Challa, S., DeBerardinis, R.J., Kraus, W.L., 2018. Metabolic regulation of transcription through compartmentalized NAD+ biosynthesis. Science 360(6389). https://doi.org/10.1126/science.aan5780.

[29] Babicki, S., Arndt, D., Marcu, A., Liang, Y., Grant, J.R., Maciejewski, A., et al., 2016. Heatmapper: web-enabled heat mapping for all. Nucleic Acids Research 44(W1):W147–W153. https://doi.org/10.1093/nar/gkw419.

[30] Chosa, M., Soeta, S., Ichihara, N., Nishita, T., Asari, M., Matsumoto, S., et al., 2009. Pathomechanism of cellular infiltration in the perivascular region of several organs in SAMP1/Yit mouse. Journal of Veterinary Medical Science 71(12):1553–1560. https://doi.org/10.1292/jvms.001553.

[31] Ehrhardt, N., Cui, J., Dagdeviren, S., Saengnipanthkul, S., Goodridge, H.S., Kim, J.K., et al., 2019. Adiposity-independent effects of aging on insulin sensitivity and clearance in mice and humans. Obesity 27(3):434–443. https://doi.org/10.1002/oby.22418.

[32] Grote, C.W., Groover, A.L., Ryals, J.M., Geiger, P.C., Feldman, E.L., Wright, D.E., 2013. Peripheral nervous system insulin resistance in ob/ob mice. Acta Neuropathologica Communications 1:1–11. https://doi.org/10.1186/2051-5960-1-15.

[33] Hedeskov, C.J., 1980. Mechanism of glucose-induced insulin secretion. Physiological Reviews 60(2):442–509. https://doi.org/10.1152/physrev.1980.60.2.442.

[34] MacDonald, M.J., 1993. Glucose enters mitochondrial metabolism via both carboxylation and decarboxylation of pyruvate in pancreatic islets. Metabolism 42(10):1229–1231. https://doi.org/10.1016/0026-0495(93)90118-8.

[35] Lenzen, S., 2014. A fresh view of glycolysis and glucokinase regulation: history and current status. Journal of Biological Chemistry 289(18):12189–12194. https://doi.org/10.1074/jbc.R114.557314.

[36] Becker, T.C., Noel, R.J., Johnson, J.H., Lynch, R.M., Hirose, H., Tokuyama, Y., et al., 1996. Differential effects of overexpressed glucokinase and hexokinase I in isolated islets: evidence for functional segregation of the high and low Km enzymes. Journal of Biological Chemistry 271(1):390–394. https://doi.org/10.1074/jbc.271.1.390.

[37] Prentki, M., Nolan, C.J., 2006. Islet β cell failure in type 2 diabetes. The Journal of Clinical Investigation 116(7):1802–1812. https://doi.org/10.1172/JCI29103.

[38] Davis, R.C., Schadt, E.E., Cervino, A.C., Péterfy, M., Lusis, A.J., 2005. Ultrafine maing of SNPs from mouse strains C57BL/6J, DBA/2J, and C57BLKS/J for loci contributing to diabetes and atherosclerosis susceptibility. Diabetes 54(4):1191–1199. https://doi.org/10.2337/diabetes.54.4.1191.

[39] Anderson, A.A., Helmering, J., Juan, T., Li, C.-M., McCormick, J., Graham, M., et al., 2009. Pancreatic islet expression profiling in diabetes-prone C57BLKS/J mice reveals transcriptional differences contributed by DBA loci, including Plagl1 and Nnt. Pathogenetics 2(1):1–17. https://doi.org/10.1186/1755-8417-2-1.

[40] Kooptiwut, S., Zraika, S., Thorburn, A.W., Dunlop, M.E., Darwiche, R., Kay, T.W., et al., 2002. Comparison of insulin secretory function in two

mouse models with different susceptibility to β-cell failure. Endocrinology 143(6):2085—2092. https://doi.org/10.1210/endo.143.6.8859.

[41] Swisa, A., Glaser, B., Dor, Y., 2017. Metabolic stress and compromised identity of pancreatic beta cells. Frontiers in Genetics 8:21. https://doi.org/10.3389/fgene.2017.00021.

[42] Bensellam, M., Jonas, J.-C., Laybutt, D.R., 2018. Mechanisms of β-cell dedifferentiation in diabetes: recent findings and future research directions. Journal of Endocrinology 236(2):R109—R143. https://doi.org/10.1530/JOE-17-0516.

[43] Hang, Y., Stein, R., 2011. MafA and MafB activity in pancreatic β cells. Trends in Endocrinology and Metabolism 22(9):364—373. https://doi.org/10.1016/j.tem.2011.05.003.

[44] Talchai, C., Xuan, S., Lin, H.V., Sussel, L., Accili, D., 2012. Pancreatic β cell dedifferentiation as a mechanism of diabetic β cell failure. Cell 150(6):1223—1234. https://doi.org/10.1016/j.cell.2012.07.029.

[45] Kim-Muller, J.Y., Fan, J., Kim, Y.J.R., Lee, S.-A., Ishida, E., Blaner, W.S., et al., 2016. Aldehyde dehydrogenase 1a3 defines a subset of failing pancreatic β cells in diabetic mice. Nature Communications 7(1):1—11. https://doi.org/10.1038/ncomms12631.

[46] Guo, S., Dai, C., Guo, M., Taylor, B., Harmon, J.S., Sander, M., et al., 2013. Inactivation of specific β cell transcription factors in type 2 diabetes. The Journal of Clinical Investigation 123(8):3305—3316. https://doi.org/10.1172/JCI65390.

[47] Cinti, F., Bouchi, R., Kim-Muller, J.Y., Ohmura, Y., Sandoval, P.R., Masini, M., et al., 2016. Evidence of β-cell dedifferentiation in human type 2 diabetes. The Journal of Clinical Endocrinology & Metabolism 101(3):1044—1054. https://doi.org/10.1210/jc.2015-2860.

[48] Zhou, X., Curbo, S., Li, F., Krishnan, S., Karlsson, A., 2018. Inhibition of glutamate oxaloacetate transaminase 1 in cancer cell lines results in altered metabolism with increased dependency of glucose. BMC Cancer 18(1):1—14. https://doi.org/10.1186/s12885-018-4443-1.

[49] Kremer, D.M., Nelson, B.S., Lin, L., Yarosz, E.L., Halbrook, C.J., Kerk, S.A., et al., 2021. GOT1 inhibition promotes pancreatic cancer cell death by ferroptosis. Nature Communications 12(1):1—13. https://doi.org/10.1038/s41467-021-24859-2.

[50] Lilla, V., Webb, G., Rickenbach, K., Maturana, A., Steiner, D.F., Halban, P.A., et al., 2003. Differential gene expression in well-regulated and dysregulated pancreatic β-cell (MIN6) sublines. Endocrinology 144(4):1368—1379. https://doi.org/10.1210/en.2002-220916.

[51] Zhao, R., Lu, J., Li, Q., Xiong, F., Zhang, Y., Zhu, J., et al., 2021. Single-cell heterogeneity analysis and CRISPR screens in MIN6 cell line reveal transcriptional regulators of insulin. Cell Cycle, 1—13. https://doi.org/10.1080/15384101.2021.1969204.

[52] Verdin, E., 2015. NAD+ in aging, metabolism, and neurodegeneration. Science 350(6265):1208—1213. https://doi.org/10.1126/science.aac4854.

[53] Solomon, J.M., Pasupuleti, R., Xu, L., McDonagh, T., Curtis, R., DiStefano, P.S., et al., 2006. Inhibition of SIRT1 catalytic activity increases p53 acetylation but does not alter cell survival following DNA damage. Molecular and Cellular Biology 26(1):28—38. https://doi.org/10.1128/MCB.26.1.28-38.2006.

[54] Milburn, J.L., Hirose, H., Lee, Y.H., Nagasawa, Y., Ogawa, A., Ohneda, M., et al., 1995. Pancreatic β-cells in obesity: evidence for induction of functional, morphologic, and metabolic abnormalities by increased long chain fatty acids. Journal of Biological Chemistry 270(3):1295—1299. https://doi.org/10.1074/jbc.270.3.1295.

[55] Cockburn, B.N., Ostrega, D.M., Sturis, J., Kubstrup, C., Polonsky, K.S., Bell, G.I., 1997. Changes in pancreatic islet glucokinase and hexokinase activities with increasing age, obesity, and the onset of diabetes. Diabetes 46(9):1434—1439. https://doi.org/10.2337/diab.46.9.1434.

[56] Zhou, Y.P., Cockburn, B.N., Pugh, W., Polonsky, K.S., 1999. Basal insulin hypersecretion in insulin-resistant Zucker diabetic and Zucker fatty rats: role of enhanced fuel metabolism. Metabolism 48(7):857—864. https://doi.org/10.1016/S0026-0495(99)90219-6.

[57] Cavaghan, M.K., Ehrmann, D.A., Polonsky, K.S., 2000. Interactions between insulin resistance and insulin secretion in the development of glucose intolerance. The Journal of Clinical Investigation 106(3):329—333. https://doi.org/10.1172/JCI10761.

[58] Omori, K., Nakamura, A., Miyoshi, H., Yamauchi, Y., Kawata, S., Takahashi, K., et al., 2021. Glucokinase inactivation paradoxically ameliorates glucose intolerance by increasing β-Cell mass in db/db mice. Diabetes 70(4):917—931. https://doi.org/10.2337/db20-0881.

[59] Liu, Y.Q., Jetton, T.L., Leahy, J.L., 2002. β-Cell adaptation to insulin resistance: increased pyruvate carboxylase and malate-pyruvate shuttle activity in islets of nondiabetic Zucker fatty rats. Journal of Biological Chemistry 277(42):39163—39168. https://doi.org/10.1074/jbc.M207157200.

[60] Irles, E., Ñeco, P., Lluesma, M., Villar-Pazos, S., Santos-Silva, J.C., Vettorazzi, J.F., et al., 2015. Enhanced glucose-induced intracellular signaling promotes insulin hypersecretion: pancreatic beta-cell functional adaptations in a model of genetic obesity and prediabetes. Molecular and Cellular Endocrinology 404:46—55. https://doi.org/10.1016/j.mce.2015.01.033.

[61] Chareyron, I., Christen, S., Moco, S., Valsesia, A., Lassueur, S., Dayon, L., et al., 2020. Augmented mitochondrial energy metabolism is an early response to chronic glucose stress in human pancreatic beta cells. Diabetologia 63(12):2628—2640. https://doi.org/10.1007/s00125-020-05275-5.

[62] Jonas, J.-C., Sharma, A., Hasenkamp, W., Ilkova, H., Patane, G., Laybutt, R., et al., 1999. Chronic hyperglycemia triggers loss of pancreatic β cell differentiation in an animal model of diabetes. Journal of Biological Chemistry 274(20):14112—14121. https://doi.org/10.1074/jbc.274.20.14112.

[63] Hayami, T., Yokoi, N., Yamaguchi, T., Honda, K., Murao, N., Takahashi, H., et al., 2020. Tumor-like features of gene expression and metabolic profiles in enlarged pancreatic islets are associated with impaired incretin-induced insulin secretion in obese diabetes: a study of Zucker fatty diabetes mellitus rat. Journal of Diabetes Investigation 11(6):1434—1447. https://doi.org/10.1111/jdi.13272.

[64] Ebrahimi, A.G., Hollister-Lock, J., Sullivan, B.A., Tsuchida, R., Bonner-Weir, S., Weir, G.C., 2020. Beta cell identity changes with mild hyperglycemia: Implications for function, growth, and vulnerability. Molecular Metabolism 35:100959. https://doi.org/10.1016/j.molmet.2020.02.002.

[65] Sun, J., Ni, Q., Xie, J., Xu, M., Zhang, J., Kuang, J., et al., 2019. β-Cell dedifferentiation in patients with T2D with adequate glucose control and nondiabetic chronic pancreatitis. The Journal of Clinical Endocrinology & Metabolism 104(1):83—94. https://doi.org/10.1210/jc.2018-00968.

[66] Amo-Shiinoki, K., Tanabe, K., Hoshii, Y., Matsui, H., Harano, R., Fukuda, T., et al., 2021. Islet cell dedifferentiation is a pathologic mechanism of long-standing progression of type 2 diabetes. JCI insight 6(1). https://doi.org/10.1172/jci.insight.143791.

[67] Kim-Muller, J.Y., Zhao, S., Srivastava, S., Mugabo, Y., Noh, H.-L., Kim, Y.R., et al., 2014. Metabolic inflexibility impairs insulin secretion and results in MODY-like diabetes in triple FoxO-deficient mice. Cell Metabolism 20(4):593—602. https://doi.org/10.1016/j.cmet.2014.08.012.

[68] Nordmann, T.M., Dror, E., Schulze, F., Traub, S., Berishvili, E., Barbieux, C., et al., 2017. The role of inflammation in β-cell dedifferentiation. Scientific Reports 7(1):1—10. https://doi.org/10.1038/s41598-017-06731-w.

[69] Sheikh-Ali, M., Sultan, S., Alamir, A.-R., Haas, M.J., Mooradian, A.D., 2010. Hyperglycemia-induced endoplasmic reticulum stress in endothelial cells. Nutrition 26(11—12):1146—1150. https://doi.org/10.1016/j.nut.2009.08.019.

[70] Robertson, R.P., 2004. Chronic oxidative stress as a central mechanism for glucose toxicity in pancreatic islet beta cells in diabetes. Journal of Biological Chemistry 279(41):42351—42354. https://doi.org/10.1074/jbc.R400019200.

[71] Laybutt, D.R., Sharma, A., Sgroi, D.C., Gaudet, J., Bonner-Weir, S., Weir, G.C., 2002. Genetic regulation of metabolic pathways in β-cells disrupted by hyperglycemia. Journal of Biological Chemistry 277(13):10912–10921. https://doi.org/10.1074/jbc.M111751200.

[72] Buteau, J., Shlien, A., Foisy, S., Accili, D., 2007. Metabolic diapause in pancreatic β-cells expressing a gain-of-function mutant of the forkhead protein Foxo1. Journal of Biological Chemistry 282(1):287–293. https://doi.org/10.1074/jbc.M606118200.

[73] Kuo, T., Kraakman, M.J., Damle, M., Gill, R., Lazar, M.A., Accili, D., 2019. Identification of C2CD4A as a human diabetes susceptibility gene with a role in β cell insulin secretion. Proceedings of the National Academy of Sciences of the United States of America 116(40):20033–20042. https://doi.org/10.1073/pnas.1904311116.

[74] Kuo, T., Du, W., Miyachi, Y., Dadi, P.K., Jacobson, D.A., Segrè, D., et al., 2021. Antagonistic epistasis of Hnf4α and FoxO1 metabolic networks through enhancer interactions in β-cell function. Molecular Metabolism 101256. https://doi.org/10.1016/j.molmet.2021.101256.

[75] Natalini, P., Ruggieri, S., Raffaelli, N., Magni, G., 1986. Nicotinamide mononucleotide adenylyltransferase. Molecular and enzymic properties of the homogeneous enzyme from bakers' yeast. Biochemistry 25(12):3725–3729. https://doi.org/10.1021/bi00360a037.

[76] Emanuelli, M., Carnevali, F., Saccucci, F., Pierella, F., Amici, A., Raffaelli, N., et al., 2001. Molecular cloning, chromosomal localization, tissue mRNA levels, bacterial expression, and enzymatic properties of human NMN adenylyltransferase. Journal of Biological Chemistry 276(1):406–412. https://doi.org/10.1074/jbc.M008700200.

[77] Berger, F., Lau, C., Dahlmann, M., Ziegler, M., 2005. Subcellular compartmentation and differential catalytic properties of the three human nicotinamide mononucleotide adenylyltransferase isoforms. Journal of Biological Chemistry 280(43):36334–36341. https://doi.org/10.1074/jbc.M508660200.

[78] Coleman, M.P., Höke, A., 2020. Programmed axon degeneration: from mouse to mechanism to medicine. Nature Reviews Neuroscience 21(4):183–196. https://doi.org/10.1038/s41583-020-0269-3.

[79] Yalowitz, J.A., Xiao, S., Biju, M.P., Antony, A.C., Cummings, O.W., Deeg, M.A., et al., 2004. Characterization of human brain nicotinamide 5′-mononucleotide adenylyltransferase-2 and expression in human pancreas. Biochemical Journal 377(2):317–326. https://doi.org/10.1042/bj20030518.

[80] Stamenkovic, J.A., Andersson, L.E., Adriaenssens, A.E., Bagge, A., Sharoyko, V.V., Gribble, F., et al., 2015. Inhibition of the malate–aspartate shuttle in mouse pancreatic islets abolishes glucagon secretion without affecting insulin secretion. Biochemical Journal 468(1):49–63. https://doi.org/10.1042/BJ20140697.

[81] Nicholls, D.G., 2016. The pancreatic β-cell: a bioenergetic perspective. Physiological Reviews 96(4):1385–1447. https://doi.org/10.1152/physrev.00009.2016.

[82] Moynihan, K.A., Grimm, A.A., Plueger, M.M., Bernal-Mizrachi, E., Ford, E., Cras-Méneur, C., et al., 2005. Increased dosage of mammalian Sir2 in pancreatic β cells enhances glucose-stimulated insulin secretion in mice. Cell Metabolism 2(2):105–117. https://doi.org/10.1016/j.cmet.2005.07.001.

[83] Ramsey, K.M., Mills, K.F., Satoh, A., Imai, S.I., 2008. Age-associated loss of Sirt1-mediated enhancement of glucose-stimulated insulin secretion in beta cell-specific Sirt1-overexpressing (BESTO) mice. Aging Cell 7(1):78–88. https://doi.org/10.1111/j.1474-9726.2007.00355.x.

[84] Wu, L., Zhou, L., Lu, Y., Zhang, J., Jian, F., Liu, Y., et al., 2012. Activation of SIRT1 protects pancreatic β-cells against palmitate-induced dysfunction. Biochimica et Biophysica Acta (BBA)-Molecular Basis of Disease 1822(11):1815–1825. https://doi.org/10.1016/j.bbadis.2012.08.009.

[85] Andrabi, S.A., Umanah, G.K., Chang, C., Stevens, D.A., Karuppagounder, S.S., Gagné, J.-P., et al., 2014. Poly (ADP-ribose) polymerase-dependent energy depletion occurs through inhibition of glycolysis. Proceedings of the National Academy of Sciences of the United States of America 111(28):10209–10214. https://doi.org/10.1073/pnas.1405158111.

[86] Fouquerel, E., Goellner, E.M., Yu, Z., Gagné, J.-P., de Moura, M.B., Feinstein, T., et al., 2014. ARTD1/PARP1 negatively regulates glycolysis by inhibiting hexokinase 1 independent of NAD+ depletion. Cell Reports 8(6):1819–1831. https://doi.org/10.1016/j.celrep.2014.08.036.

[87] Yabuki, A., Maeda, M., Matsumoto, M., Kamimura, R., Masuyama, T., Suzuki, S., 2005. SAMP1/Sku as a murine model for tubulointerstitial nephritis: a study using unilateral ureteral obstruction. Experimental Animals 54(1):53–60. https://doi.org/10.1538/expanim.54.53.

[88] Niimi, K., Takahashi, E., Itakura, C., 2009. Adiposity-related biochemical phenotype in senescence-accelerated mouse prone 6 (SAMP6). Comparative Medicine 59(5):431–436.

[89] Robertson, R.P., Harmon, J.S., 2006. Diabetes, glucose toxicity, and oxidative stress: a case of double jeopardy for the pancreatic islet β cell. Free Radical Biology and Medicine 41(2):177–184. https://doi.org/10.1016/j.freeradbiomed.2005.04.030.

[90] Kajimoto, Y., Kaneto, H., 2004. Role of oxidative stress in pancreatic β-cell dysfunction. In: Lee, H.K., DiMauro, S., Tanaka, M., Wei, Y.H. (Eds.), Mitochondrial pathogenesis. Springer. p. 168–76. https://doi.org/10.1007/978-3-662-41088-2_17.

[91] Liguori, I., Russo, G., Curcio, F., Bulli, G., Aran, L., Della-Morte, D., et al., 2018. Oxidative stress, aging, and diseases. Clinical Interventions in Aging 13:757. https://doi.org/10.2147/CIA.S158513.

[92] Barquissau, V., Capel, F., Dardevet, D., Feillet-Coudray, C., Gallinier, A., Chauvin, M.-A., et al., 2017. Reactive oxygen species enhance mitochondrial function, insulin sensitivity and glucose uptake in skeletal muscle of senescence accelerated prone mice SAMP8. Free Radical Biology and Medicine 113:267–279. https://doi.org/10.1016/j.freeradbiomed.2017.10.012.

[93] Haythorne, E., Rohm, M., van de Bunt, M., Brereton, M.F., Tarasov, A.I., Blacker, T.S., et al., 2019. Diabetes causes marked inhibition of mitochondrial metabolism in pancreatic β-cells. Nature Communications 10(1):1–17. https://doi.org/10.1038/s41467-019-10189-x.

[94] Jukarainen, S., Heinonen, S., Rämö, J.T., Rinnankoski-Tuikka, R., Ra:ou, E., Tummers, M., et al., 2016. Obesity is associated with low NAD+/SIRT pathway expression in adipose tissue of BMI-discordant monozygotic twins. The Journal of Clinical Endocrinology & Metabolism 101(1):275–283. https://doi.org/10.1210/jc.2015-3095.

[95] Xu, H., Barnes, G.T., Yang, Q., Tan, G., Yang, D., Chou, C.J., et al., 2003. Chronic inflammation in fat plays a crucial role in the development of obesity-related insulin resistance. The Journal of Clinical Investigation 112(12):1821–1830. https://doi.org/10.1172/JCI19451.

[96] Halter, J.B., 2011. Aging and insulin secretion. In: Masoro, E.J., Austad, S.N. (Eds.), Handbook of the biology of aging. Elsevier. p. 373–84. https://doi.org/10.1016/B978-0-12-378638-8.00017-8.

[97] Gumbiner, B., Polonsky, K.S., Beltz, W.F., Wallace, P., Brechtel, G., Fink, R.I., 1989. Effects of aging on insulin secretion. Diabetes 38(12):1549–1556. https://doi.org/10.2337/diab.38.12.1549.

[98] Iozzo, P., Beck-Nielsen, H., Laakso, M., Smith, U., Yki-Järvinen, H., Ferrannini, E., 1999. Independent influence of age on basal insulin secretion in nondiabetic humans. The Journal of Clinical Endocrinology & Metabolism 84(3):863–868. https://doi.org/10.1210/jcem.84.3.5542.

[99] Ihm, S.-H., Matsumoto, I., Sawada, T., Nakano, M., Zhang, H.J., Ansite, J.D., et al., 2006. Effect of donor age on function of isolated human islets. Diabetes 55(5):1361–1368. https://doi.org/10.2337/db05-1333.

[100] Weir, G.C., Laybutt, D.R., Kaneto, H., Bonner-Weir, S., Sharma, A., 2001. Beta-cell adaptation and decompensation during the progression of diabetes. Diabetes 50(Suppl 1):S154. https://doi.org/10.2337/diabetes.50.2007.s154.

 www.molecularmetabolism.com